





Subcellular localization of Type VI secretion system assembly in response to cell–cell contact

Lin Lin¹ , Raffaella Capozzoli¹, Alexia Ferrand² , Miro Plum¹, Andrea Vettiger^{1,†}  & Marek Basler^{1,*} 

Abstract

Bacteria require a number of systems, including the type VI secretion system (T6SS), for interbacterial competition and pathogenesis. The T6SS is a large nanomachine that can deliver toxins directly across membranes of proximal target cells. Since major reassembly of T6SS is necessary after each secretion event, accurate timing and localization of T6SS assembly can lower the cost of protein translocation. Although critically important, mechanisms underlying spatiotemporal regulation of T6SS assembly remain poorly understood. Here, we used super-resolution live-cell imaging to show that while *Acinetobacter* and *Burkholderia thailandensis* can assemble T6SS at any site, a significant subset of T6SS assemblies localizes precisely to the site of contact between neighboring bacteria. We identified a class of diverse, previously uncharacterized, periplasmic proteins required for this dynamic localization of T6SS to cell–cell contact (TslA). This precise localization is also dependent on the outer membrane porin OmpA. Our analysis links transmembrane communication to accurate timing and localization of T6SS assembly as well as uncovers a pathway allowing bacterial cells to respond to cell–cell contact during interbacterial competition.

Keywords cell–cell contact; cell–surface contact; dynamic localization; structured illumination microscopy; type VI secretion

Subject Categories Membranes & Trafficking; Microbiology, Virology & Host Pathogen Interaction

DOI 10.15252/embj.2021108595 | Received 28 April 2021 | Revised 18 April 2022 | Accepted 29 April 2022 | Published online 30 May 2022

The EMBO Journal (2022) 41: e108595

Introduction

Microorganisms often co-exist in close contact with one another and compete for limited resources. The mechanisms involved in competition can be contact independent or contact dependent. Contact-independent competition relies on the secretion of antimicrobial

molecules into the environment (Michel-Briand & Baysse, 2002; Cascales *et al.*, 2007; Cornforth & Foster, 2013). Certain toxins may be delivered into neighboring cells in a contact-dependent manner by various secretion systems. Such secretion systems include subtypes of the Type IV secretion systems (Souza *et al.*, 2015; Sgro *et al.*, 2018, 2019), the Type V secretion system for contact-dependent growth inhibition (Aoki *et al.*, 2005, 2009; Garcia, 2018), and the Type VI secretion system (T6SS) (Pukatzki *et al.*, 2006).

T6SS is a widespread secretion system found in Gram-negative bacteria that deliver effector proteins into the adjacent eukaryotic or bacterial cells (Bingle *et al.*, 2008; Durand *et al.*, 2014; Russell *et al.*, 2014a; Diniz *et al.*, 2015; Hachani *et al.*, 2016). The T6SS structurally resembles an inverted contractile phage tail-like structure (Pukatzki *et al.*, 2007; Leiman *et al.*, 2009; Basler *et al.*, 2012; Wang *et al.*, 2019). T6SS assembly is initiated by the formation of a membrane complex comprising TssL, TssM, and often TssJ proteins anchored to the cell envelope (Ma *et al.*, 2009, 2012; Aschtgen *et al.*, 2010; Felisberto-Rodrigues *et al.*, 2011; Durand *et al.*, 2012, 2015; Yin *et al.*, 2019). A baseplate complex composed of effector decorated VgrG/PAAR spike and TssEFGK forms on the membrane complex and initiates copolymerization of the contractile sheath (TssBC) and the inner Hcp tube (Basler *et al.*, 2012; Zoued *et al.*, 2013; Kudryashev *et al.*, 2015; Filloux & Freemont, 2016; Vettiger *et al.*, 2017; Wang *et al.*, 2017; Cherrak *et al.*, 2018; Nazarov *et al.*, 2018; Park *et al.*, 2018). Upon an unknown signal, the extended sheath contracts and propels the inner Hcp tube, VgrG/PAAR, and effectors into the environment or a neighboring cell (Basler *et al.*, 2012; Szwedziak & Pilhofer, 2019). Upon sheath contraction, an ATPase ClpV or ClpB binds the contracted sheath and unfolds the sheath subunits, allowing new rounds of T6SS assembly (Bönemann *et al.*, 2009; Pietrosiuk *et al.*, 2011; Basler & Mekalanos, 2012; Basler *et al.*, 2012; Kapitein *et al.*, 2013; Förster *et al.*, 2014; Brodmann *et al.*, 2017).

Despite the conservation of its overall structure, the T6SS exhibits diverse assembly dynamics in different bacterial species. In some strains of *Vibrio cholerae*, an average of 2–5 T6SS structures per cell are randomly assembled during exponential growth (Vettiger *et al.*, 2017; Lin *et al.*, 2019). On the other hand, in *Francisella novicida*, which requires T6SS to escape from macrophages, T6SS assembly preferentially occurs at the bacterial cell pole (Brodmann

¹ Biozentrum, University of Basel, Basel, Switzerland

² Biozentrum, Imaging Core Facility, University of Basel, Basel, Switzerland

*Corresponding author. Tel: +41 61 207 21 10; E-mail: marek.basler@unibas.ch

[†]Present address: Department of Microbiology, Blavatnik Institute, Harvard Medical School, Boston, MA, USA

et al, 2017). Similarly, the T6SS-5 of *Burkholderia thailandensis*, which is required for formation of multinucleated giant cells, also assembles at the cell pole (Schwarz et al, 2014). The biological significance and the mechanism of this spatial and temporal regulation are unknown.

Most studies of T6SS localization have been conducted on the H1-T6SS from *Pseudomonas aeruginosa*. H1-T6SS assembles upon T6SS attack from the neighboring cells or upon sensing membrane damage (Basler et al, 2013; Ho et al, 2013; Kamal et al, 2020). This response is regulated by phosphorylation of the T6SS component Fha by PpkA kinase, a process reversed by the PppA phosphatase (Mougous et al, 2007). This threonine phosphorylation pathway uses a sensor module in the membrane consisting of TagQRST, which activates PpkA through an unknown mechanism (Hsu et al, 2009; Casabona et al, 2013; Wang et al, 2019). In addition, a repressor TagF has been shown to sequester Fha to repress T6SS assembly in *P. aeruginosa* (Silverman et al, 2011; Lin et al, 2018). Indeed, *tagF* deletion leads to T6SS activation independent of the presence of TagQRST and PpkA (Silverman et al, 2011). Importantly, this dynamic localization and repeated assembly of T6SS in *P. aeruginosa* likely evolved to allow efficient killing of target cells (Basler et al, 2013; Smith et al, 2020).

Recently, posttranslational regulation of T6SS has also been reported in species like *Agrobacterium tumefaciens* and *Serratia marcescens*. Interestingly, PpkA/PppA/Fha components are present, while the sensor module TagQRST is absent in these species (Fritsch et al, 2013; Lin et al, 2014; Gerc et al, 2015; Ostrowski et al, 2018). However, in *A. tumefaciens*, TagF domain and PppA form a chimeric protein and block T6SS assembly by interacting with Fha (Lin et al, 2014, 2018), while in *S. marcescens* TagF blocks the membrane complex assembly (Ostrowski et al, 2018). In addition, in some organisms, specialized peptidoglycan-modifying enzymes have been linked to initiation of T6SS assembly. For example, the lytic transglycosylase MltE in enteroaggregative *Escherichia coli* (EAEC) interacts with the periplasmic domain of TssM, which stimulates MltE activity (Santin & Cascales, 2017). Localized MltE-mediated peptidoglycan degradation then allows membrane complex assembly by promoting TssM oligomerization (Santin & Cascales, 2017). Similarly, in *Acinetobacter*, an L, D-endopeptidase TagX is important for the T6SS activity, Hcp secretion, and killing of prey cells (Weber et al, 2016; Ringel et al, 2017). Thus, while we have some insight into T6SS regulation, how

these mechanisms relate to precise spatial and temporal regulation of assembly remains unclear.

Here, we used structured illumination microscopy (SIM) to investigate the subcellular localization of antibacterial T6SS in gammaproteobacteria *Acinetobacter baylyi* and *Acinetobacter baumannii*, as well as betaproteobacteria *B. thailandensis*. We identified two different modes of T6SS assembly in these species: one localized to cell-cell contact sites and one contact independent. Contact-dependent assembly is initiated by localized assembly of a small sheath focus, which is later extended to a full-length sheath. We further show that contact-dependent assembly depends on a periplasmic protein that we name Type six secretion dynamic localization protein A (TslA). Furthermore, our data suggest that the outer membrane porin OmpA is important for contact-dependent T6SS assembly, establishing a link between the outer membrane and initiation of T6SS assembly in the periplasm.

Results

T6SS frequently assembles at the site of contact with a neighboring cell

To gain insight into the mechanisms underlying T6SS assembly in *A. baylyi*, we used 3D-structured illumination microscopy (SIM) and followed localization of the sheath component TssB tagged with superfolder GFP (TssB-sfGFP) (Fig 1A and Movie EV1). As previously observed (Ringel et al, 2017), the *A. baylyi* T6SS sheath polymerizes at a rate of 36 ± 9 nm/s ($n = 300$). Sheaths assembled on average in about 22 ± 7 s ($n = 63$). The sheath often buckled right before contraction, and contracted immediately after assembling across the whole cell (Fig EV1A). Contracted sheaths were disassembled in 65 ± 22 s ($n = 63$). Interestingly, about 50% of sheaths (156 of 300) contracted away from the baseplate (Fig EV1B), similarly as previously reported in *E. coli* (Szwedziak & Pilhofer, 2019). Importantly, higher resolution of 3D-SIM revealed that TssB-sfGFP formed multiple small foci at the cell periphery (Fig 1A and C). Additionally, in a dense population, where many cells are in close contact with each other, about one third of sheaths ($33.48 \pm 2.09\%$, three biological replicates) were formed at the site where the cell was in a close contact with an adjacent cell (Fig 1A

Figure 1. Super-resolution imaging of T6SS by 3D-SIM reveals the formation of sheath foci prior to sheath polymerization.

- A Time-lapse 3D-SIM of T6SS assembly, contraction, and disassembly by visualizing TssB-sfGFP in *A. baylyi*. Yellow arrows indicate examples of contact-dependent T6SS assembly pairs. A larger field of view is shown in the first field of Movie EV1.
- B Scheme representing that contact-dependent and -independent T6SS assemblies occur within the cells in close contact with each other.
- C Examples of two modes of T6SS assembly in *A. baylyi* revealed by 3D-SIM live-cell imaging. Upper panel: an example of contact-dependent T6SS dynamics indicated by a green arrow; lower panel: an example of contact-independent T6SS dynamics indicated by an orange arrow.
- D Violin plots showing the distribution of sheath polymerization speed for both modes of T6SS assemblies. A total of 300 assemblies (100 from each biological replicate; 3 biological replicates) were analyzed over at least 3 min at 5 s intervals. The central dash line indicates the median while the upper and lower dash lines indicate the quartiles. Unpaired *t*-test was performed (ns, not significant).
- E Time-lapse 3D-SIM imaging of sheath dynamics (TssB-sfGFP) in the absence of membrane complex protein TssM.
- F Time-lapse 3D-SIM imaging of sheath dynamics (TssB-sfGFP) in the absence of TagX. Yellow arrows indicate examples of contact-dependent T6SS sheath foci pairs. Larger field of view is shown as the first field of Movie EV2.
- G Time-lapse 2D-SIM imaging of TssA and sheath dynamics. Imaging was performed on cells of the double-tagged strain (*tssB-mCherry2 mNeonGreen-tssA*) by 2D-SIM. White arrow indicates an example of paired T6SS assembly. Larger field of view is shown as the first field of Movie EV3.

Data information: Scale bars and time intervals are indicated.

Source data are available online for this figure.

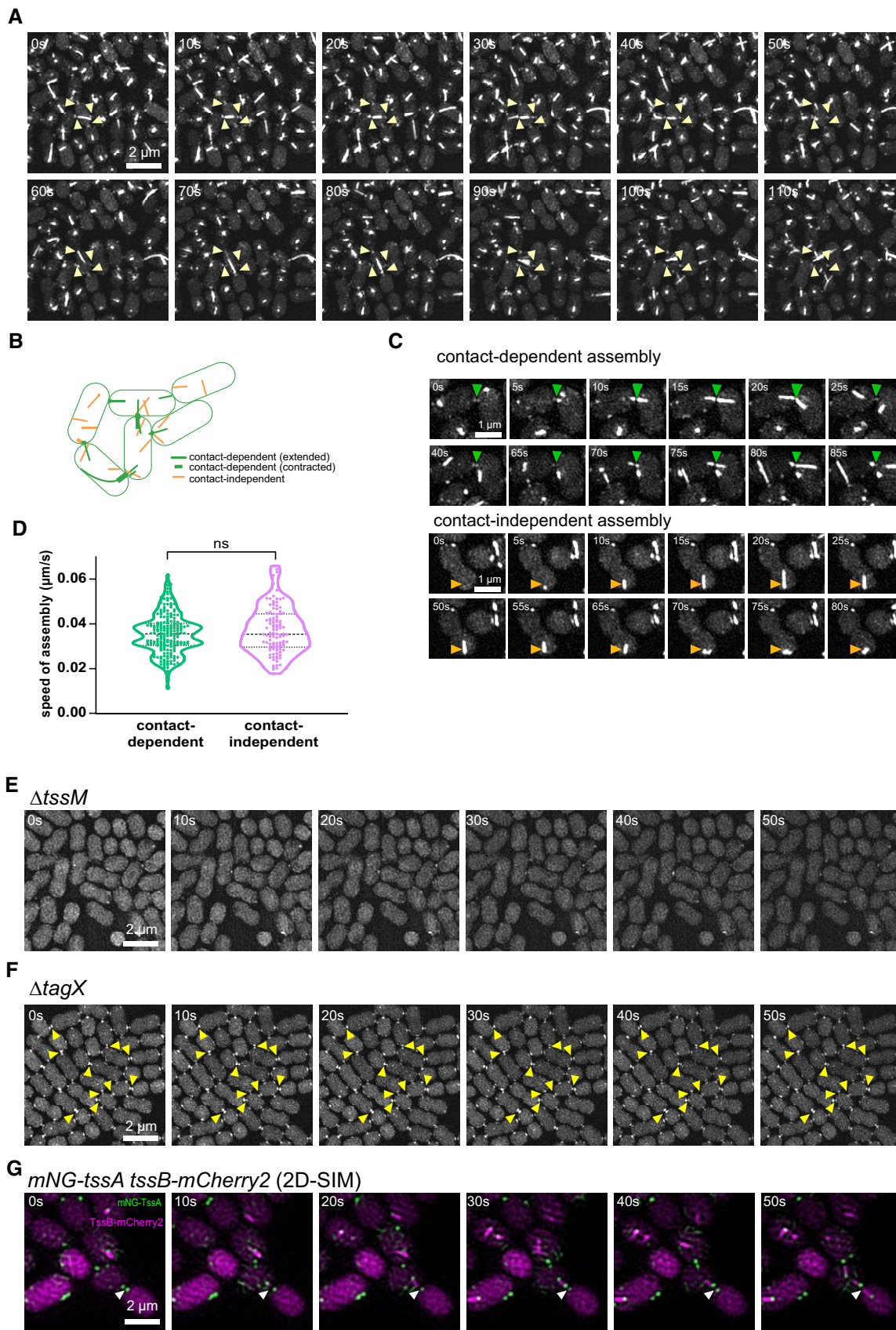


Figure 1.

and B). Moreover, the sheath foci at the cell–cell contact site often appeared as “pairs” in both of the adjacent cells (Fig 1C, upper panel). Importantly, full-length sheaths were often assembled from sheath foci with a speed that was independent of the foci localization (Fig 1D). In summary, 3D-SIM revealed that sheath assembly in *A. baylyi* is a two-step process and that about one third of the assembled T6SS localize to cell–cell contact sites while two thirds are localized without a clear pattern.

Formation of sheath foci depends on membrane complex and baseplate components but is independent of TssA and TagX

To further examine the formation of sheath foci, we analyzed TssB-sfGFP localization in the absence of the membrane complex components TssL and TssM, baseplate components TssK, TssF, and TssG, as well as TssA and TagX, known to be required for efficient initiation of T6SS assembly in *A. baylyi* (Weber et al, 2016; Ringel et al, 2017). Importantly, sheath foci were absent in *tssL*, *tssM*, *tssK*, *tssF*, and *tssG* mutants, indicating that the membrane complex and baseplate are crucial for their formation (Figs 1E and EV1C). On the other hand, we observed stable sheath foci pairs at the cell–cell contact site in the absence of *tagX*, despite a significant decrease in the assembly of full-length sheaths (Fig 1F and Movie EV2).

TssA in *A. baylyi* was shown to be important for T6SS activity as its deletion abolished the Hcp secretion (Weber et al, 2016). Interestingly, in the absence of *tssA*, sheath foci were formed and localized to the sites of cell–cell contact (Fig EV1C). To further elucidate the role of TssA in assembly of sheath foci, we tagged TssA with mNeonGreen and TssB with mCherry2 and followed their localization using 2D-SIM. Similar to TssA in *E. coli* or *V. cholerae* (Santin et al, 2018; Schneider et al, 2019), *A. baylyi* TssA colocalized with the distal end of the polymerizing sheath until contraction (Fig 1G and Movie EV3). Interestingly, we observed that TssA foci also appeared as a pair at the site of contact between two adjacent cells (Fig 1G) and thus localize similarly to sheath foci. In addition, TssA foci formed repeatedly at the same site of cell–cell contact, suggesting possible repeated T6SS assembly events at the same location (Movie EV3). Taken together, our data suggest that formation of sheath foci depends on assembled membrane complex and baseplate, but is independent of TagX and TssA. In addition, the sheath foci are likely interacting with TssA for a significant amount of time before sheath polymerization starts.

Close proximity between cells is crucial for contact-dependent assembly

Pseudomonas aeruginosa was previously shown to localize assembly of H1-T6SS to the site of membrane damage and to engage in rounds of spatially and temporally correlated T6SS assembly to attack neighboring cells (Basler et al, 2013; Ho et al, 2013; Smith et al, 2020). While localization of T6SS assembly in *A. baylyi* resembles this correlated assembly to some extent, T6SS dynamics in *A. baylyi* must be regulated by a different mechanism as the *A. baylyi* genome lacks TagQRST and Fha/PpkA/PppA homologues. Moreover, stable sheath foci occurred at cell–cell contact sites in TagX mutant that mostly lack dynamic sheaths (Fig 1F), indicating that *A. baylyi* cells respond to contact with, rather than attack from, neighboring cells. To further test this, we mixed *E. coli* MG1655

with *A. baylyi* strain lacking all known effectors required for prey killing. Previous study has shown that the absence of these effectors in *A. baylyi* abolishes killing of *E. coli* while having no effect on the frequency of T6SS assembly (Ringel et al, 2017). After 2 h of co-incubation, we monitored TssB-sfGFP dynamics in *A. baylyi*, finding that established sheath foci and subsequent assemblies of full-length sheaths occurred at the site of contact with *E. coli* cells (Fig 2A and Movie EV4). In addition, sheath foci at the contact site with *E. coli* cells also formed in *tagX* deletion mutant (Fig 2B).

To investigate how the distance between neighboring cells affects contact-dependent assembly, we determined sheath formation dynamics in the *A. baylyi* BD4 strain, which produces more capsule than *A. baylyi* ADP1 (Heidelberger et al, 1969; Juni & Janik, 1969; Juni, 1972; Patel et al, 1975). Indeed, there were gaps (~220 nm) between cells of *A. baylyi* BD4 while no such large gaps were detectable in *A. baylyi* ADP1 or BD4 mutants lacking *galU*, a factor required for capsule production (Fig EV2A). The frequency of sheath assembly in the *A. baylyi* BD4 was slightly lower (0.62 ± 0.09 sheaths per cell per min, three biological replicates) than that in the *A. baylyi* ADP1 strain (0.76 ± 0.24 sheaths per cell per min; three biological replicates). Importantly, we observed significant decrease in assemblies of sheaths or sheath foci at the site of cell–cell contact in *A. baylyi* BD4 ($2.88 \pm 1.67\%$, three biological replicates, Fig 2C and Movie EV5, left panel) or its *AtagX* mutant (Fig 2D). The frequency of contact site sheath assembly was restored in the *A. baylyi* BD4 *galU* mutant ($32.96 \pm 0.32\%$, three biological replicates; Fig EV2B and Movie EV5, right panel). Together, this shows that capsule production prevents T6SS assembly specifically at the contact sites and suggests that close contact between the outer membranes of the neighboring cells may initiate T6SS assembly.

Periplasmic protein TslA is required for contact site assembly

Several genes in the *A. baylyi* T6SS gene cluster are poorly characterized and their function is mostly unknown (Weber et al, 2016; Ringel et al, 2017) (Fig 3A). To test if these genes are required for T6SS assembly at the cell–cell contact site, we monitored TssB-sfGFP localization using 3D-SIM in strains lacking T6SS components *tagN* (ACIAD2682), *tagF* (ACIAD2683), ACIAD2685, ACIAD2693, or ACIAD2698. The deletion of *tagN*, *tagF*, or ACIAD2698 resulted in no significant change in frequency or localization of the sheath or sheath foci. However, ACIAD2685 deletion greatly reduced the frequency of full-length sheath assembly, although sheath foci still localized to cell–cell contact sites (Fig EV3A).

Surprisingly, ACIAD2693 deletion, shown previously to lead to ~50% reduction in T6SS assembly rate (Ringel et al, 2017), abolished T6SS assembly at the cell–cell contact sites as documented by the lack of paired assemblies (Fig 3B and Movie EV6, left panel). SIM imaging revealed that there were on average 0.31 ± 0.03 sheath structures assembled per cell per min, which is less than 0.76 ± 0.24 in the parental strain (Fig 3D; *t*-test, $P = 0.0318$). Out of these assemblies, only $2.59 \pm 0.76\%$ (three biological replicates) potentially originated from sites of cell–cell contact (Fig 3B and D). This is in contrast to ~33% of assemblies being localized to cell–cell contact sites in the parental strain (Fig 3D; *t*-test, $P < 0.0001$). In addition, almost no sheath foci localized at cell–cell contact sites in cells lacking ACIAD2693 (Fig 3B). Moreover, the pairs of sheath foci at the contact site between sister or prey cells were also absent in

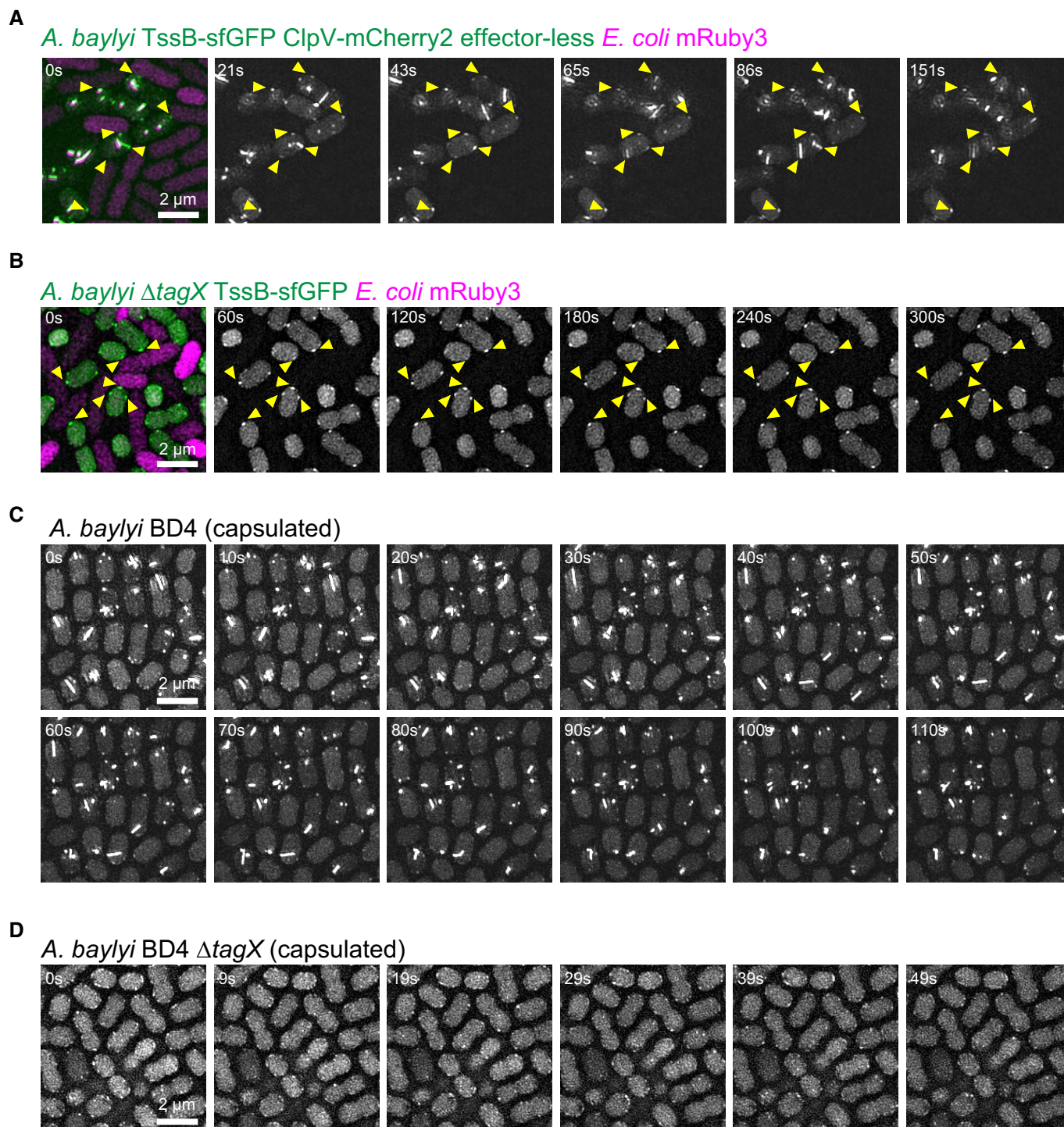


Figure 2. Close cell–cell contact is required for contact-dependent T6SS assembly.

A T6SS assembly in *A. baylyi* cells that are in contact with *E. coli*. T6SS⁺ *A. baylyi* cells lacking all known effectors (Δ Effectors *tssB-sfGFP clpV-mCherry2*) were mixed with *E. coli* cells (MG1655 *P_{tac}-mRuby3*) and incubated on LB agar plate for 2 h before imaging. Yellow arrows indicate sheath foci that are formed at the contact site with *E. coli*. An overlay of green and red fluorescence channels shown for time 0s; the time lapse for the green channel shown in grayscale. Larger field of view is shown as the third field of Movie EV4.

B Stable sheath foci formation in *A. baylyi* cells that are in contact with *E. coli*. *A. baylyi* cells lacking TagX (Δ *tagX tssB-sfGFP*) were mixed well with cells of *E. coli* (MG1655 *P_{tac}-mRuby3*) and incubated on an LB agar plate for at least 90 min before imaging. Yellow arrows indicate sheath foci that are stably present at the contact site with *E. coli*. An overlay of green and red fluorescence channels shown for time 0s; the time lapse for the green channel shown in grayscale.

C Time-lapse 3D-SIM imaging of sheath dynamics (TssB-sfGFP) in capsulated *A. baylyi* BD4 cells. Larger field of view is shown as the first field of Movie EV5.

D Time-lapse 3D-SIM imaging of sheath dynamics (TssB-sfGFP) in capsulated *A. baylyi* BD4 cells lacking TagX.

Data information: Scale bars and time intervals are indicated.

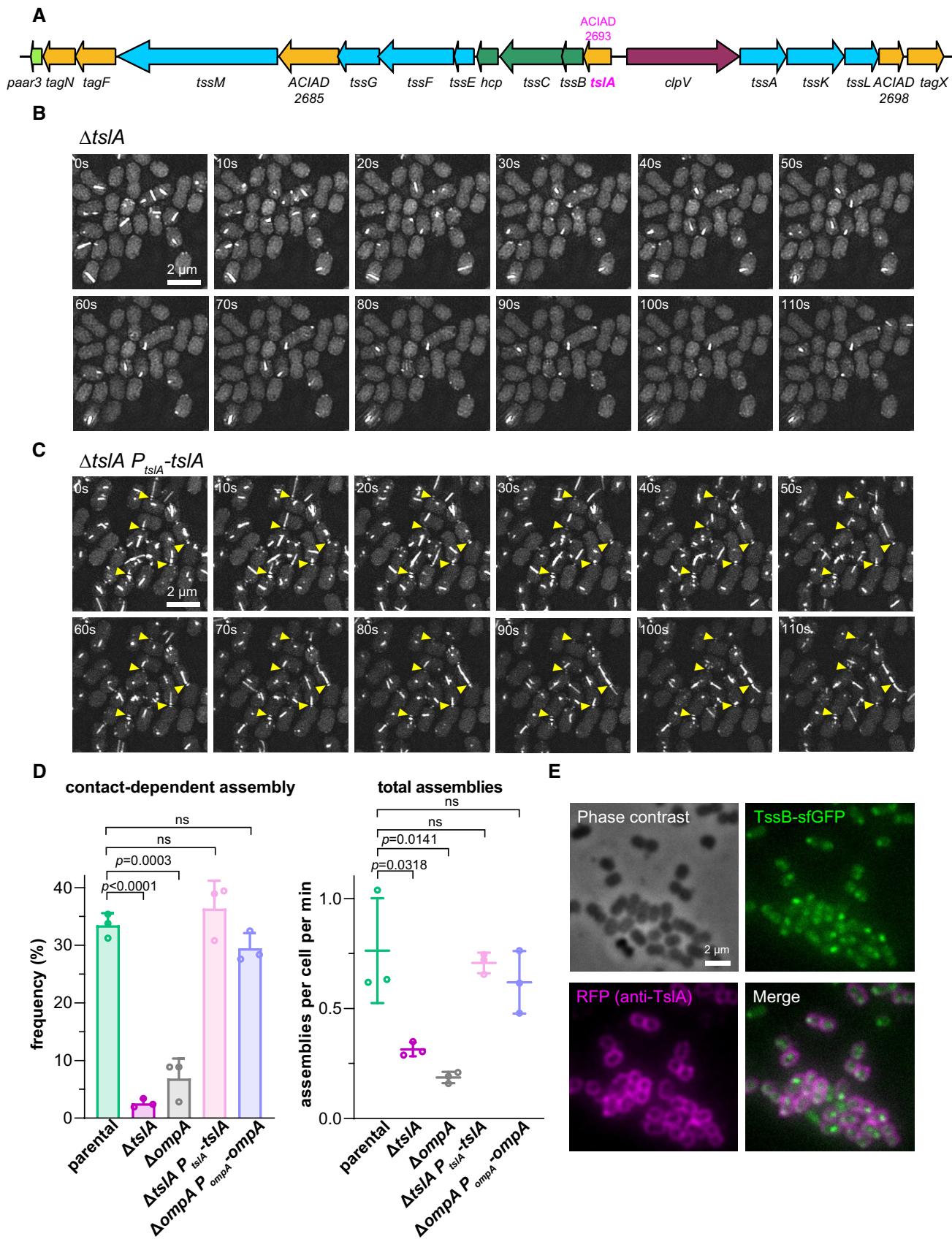


Figure 3.

Figure 3. A periplasmic protein, TslA, is important for contact-dependent T6SS assembly in *A. baylyi*.

- A Main T6SS cluster of *A. baylyi*. Genes marked in yellow are encoding proteins with unknown functions.
- B Time-lapse 3D-SIM imaging of sheath dynamics (TssB-sfGFP) in the absence of TslA. Larger field of view is shown as the third field of Movie EV6, left panel.
- C Time-lapse 3D-SIM imaging of sheath dynamics (TssB-sfGFP) in *ΔtslA* strain with ectopically expressed *tslA* (*tssB-sfGFP clpV-mCherry2 ΔtslA ampC::P_{tslA}-tslA-Kan^R*). Larger field of view is shown as the first field of Movie EV6, right panel. Yellow arrows indicate examples of contact-dependent sheath assembly.
- D The frequency of contact-dependent assembly (left panel) and number of assemblies per cell per min (right panel) in cells from different strains as indicated on X-axis. Three biological replicates were performed for each strain. At least 500 cells were analyzed per replicate on 3D-SIM time-lapse imaging of sheath dynamics (TssB-sfGFP) in 3-min period. Bar graph (left panel) and scatter dot plot (right panel) show mean \pm SD. Unpaired t-test was performed.
- E Cellular localization of TslA in *A. baylyi* cells. Cells of the strain (*tssB-sfGFP*) were fixed by 2% paraformaldehyde and treated with GTE buffer, then probed with anti-TslA antibodies, followed by incubation with secondary antibodies conjugated with Alexa Fluor Plus 594. Signals were detected using a widefield microscope. Phase contrast, GFP, RFP, and merged images are shown (GFP: TssB; RFP: TslA).

Data information: Scale bars and time intervals are indicated.

Source data are available online for this figure.

the double mutant lacking ACIAD2693 and *tagX* (Fig EV3B and C and Movie EV7, left panel).

To exclude the possibility of a polar effect of ACIAD2693 deletion on the expression of downstream genes, we ectopically expressed ACIAD2693 from a neutral site on the chromosome under its native promoter. Such ectopic expression fully restored the frequency of sheath assembly (0.71 ± 0.05 sheaths per cell per min, three biological replicates) and the sheath assembly at the cell–cell contact sites ($36.38 \pm 4.84\%$, three biological replicates, Fig 3C and D and Movie EV6, right panel). Similarly, the ectopic expression of ACIAD2693 also restored the formation of localized sheath foci pairs in Δ ACIAD2693 Δ *tagX* (Fig EV3D and Movie EV7, right panel).

ACIAD2693 has a predicted N-terminal signal peptide with the cleavage site between Ala22 and Ala23. C-terminal fusions of ACIAD2693 to mNeonGreen or mCherry2 failed to complement the deletion strain suggesting that fluorescent protein tags interfere with either protein localization or function. Therefore, to determine the subcellular localization of ACIAD2693, we performed immunofluorescence labeling using a rabbit primary antibody raised against the periplasmic part of ACIAD2693 (GeneScript) and Alexa Fluor Plus 594-labeled anti-rabbit secondary antibody (Invitrogen). This showed that ACIAD2693 specifically localizes to the periphery of *A. baylyi* (Fig 3E). Importantly, the deletion of the signal peptide led to a loss of peripheral localization and a reduction in the contact-dependent sheath assembly ($4.22 \pm 0.49\%$, three biological replicates, Fig EV3E and F). Together, our data suggest that ACIAD2693 is a periplasmic protein that is required for contact-dependent T6SS assembly, and we renamed it to Type six secretion dynamic localization protein A (TslA).

OmpA plays an important role in contact-dependent T6SS assembly

The outer membrane (OM) of Gram-negative bacteria contains many β -barrel proteins (OMPs), which are crucial for OM functions including nutrient uptake, adhesion, and the stress response (Klebb & Newton, 1998; Wimley, 2003; Laubacher & Ades, 2008; Cho et al, 2014; Heras et al, 2014). The assembly and integration of OMPs requires the β -barrel assembly machinery (BAM) (Wu et al, 2005; Sklar et al, 2007; Konovalova et al, 2017). To test if OMPs are involved in T6SS assembly, we used SIM imaging to analyze TssB localization in the absence of several OM-related proteins including non-essential components of BAM complexes. Our data do not suggest that BamB, BamC, or OmpH play a significant role in T6SS contact-dependent assembly (Fig EV4A and Movie EV8). On the other hand, the absence of BamE led to a slight reduction in overall assembly rate

(0.48 ± 0.07 sheaths per cell per min) as well as contact-dependent assembly frequency ($28.94 \pm 3.85\%$, three biological replicates).

Interestingly, we observed a significant change in T6SS dynamics in the absence of OmpA (Fig 4A and Movie EV9, left panel), one of the most abundant OMPs in *E. coli* (Li et al, 2014). The frequency of T6SS assembly was reduced to about one fourth in the absence of OmpA (0.19 ± 0.03 sheaths per cell per min in comparison to ~ 0.76 in parental strain) (Fig 4A and Movie EV9, left panel; Fig 3D; t-test, $P = 0.0141$). Moreover, contact-dependent assembly decreased from $\sim 33\%$ in the parental strain to $6.87 \pm 3.49\%$ in the *ompA* deletion strain (three biological replicates; Fig 3D; t-test, $P = 0.0003$). Finally, formation of sheath foci at the site of cell–cell contact was also decreased in the mutant lacking both OmpA and TagX (Fig 4B). Ectopic expression of *ompA* restored the contact-dependent assembly of T6SS and sheath foci thus excluding the possibility that *ompA* deletion changed expression of the downstream genes ($29.50 \pm 2.63\%$, three biological replicates, Figs 3D and EV4B and C, and Movie EV9, right panel).

As OmpA is non-covalently associated with peptidoglycan (Reusch, 2012; Confer & Ayalew, 2013), we further tested if the peptidoglycan-binding domain of OmpA is important for its role in contact-dependent T6SS assembly. We mutated to alanine two conserved residues (D273 and R288) that were shown to be essential for PG binding of OmpA (Park et al, 2012; Skerniškytė et al, 2019). The D273A+R288A mutation indeed lowered the overall rate of sheath assembly (0.27 ± 0.05 sheaths per cell per min) as well as contact-dependent assembly ($12.42 \pm 2.82\%$, three biological replicates; Fig 4C). However, it should be noted that an immunoblot analysis revealed that these point mutations partially lowered OmpA protein level in the cell lysate, indicating that PG binding may be required for OmpA stability (Fig EV4D).

In summary, since the absence of several BAM complex proteins has no effect on contact-dependent T6SS assembly, our data indicate that it is OmpA itself, rather than an overall change in OM integrity, that is important for T6SS assembly at the cell–cell contact site, however, it remains unclear if binding of OmpA to PG is required for this function.

Contact-dependent T6SS assembly in *Acinetobacter baumannii*

To test the generality of the observation of step-wise sheath assembly and precise T6SS localization, we examined assembly of T6SS in *A. baumannii*. The sequence alignment suggests that TslA homolog in *A. baumannii* DSM30011 (Wilhelm et al, 2013) or A118 (Merkier & Centrón, 2006; Ramirez et al, 2010) shares only 48% sequence

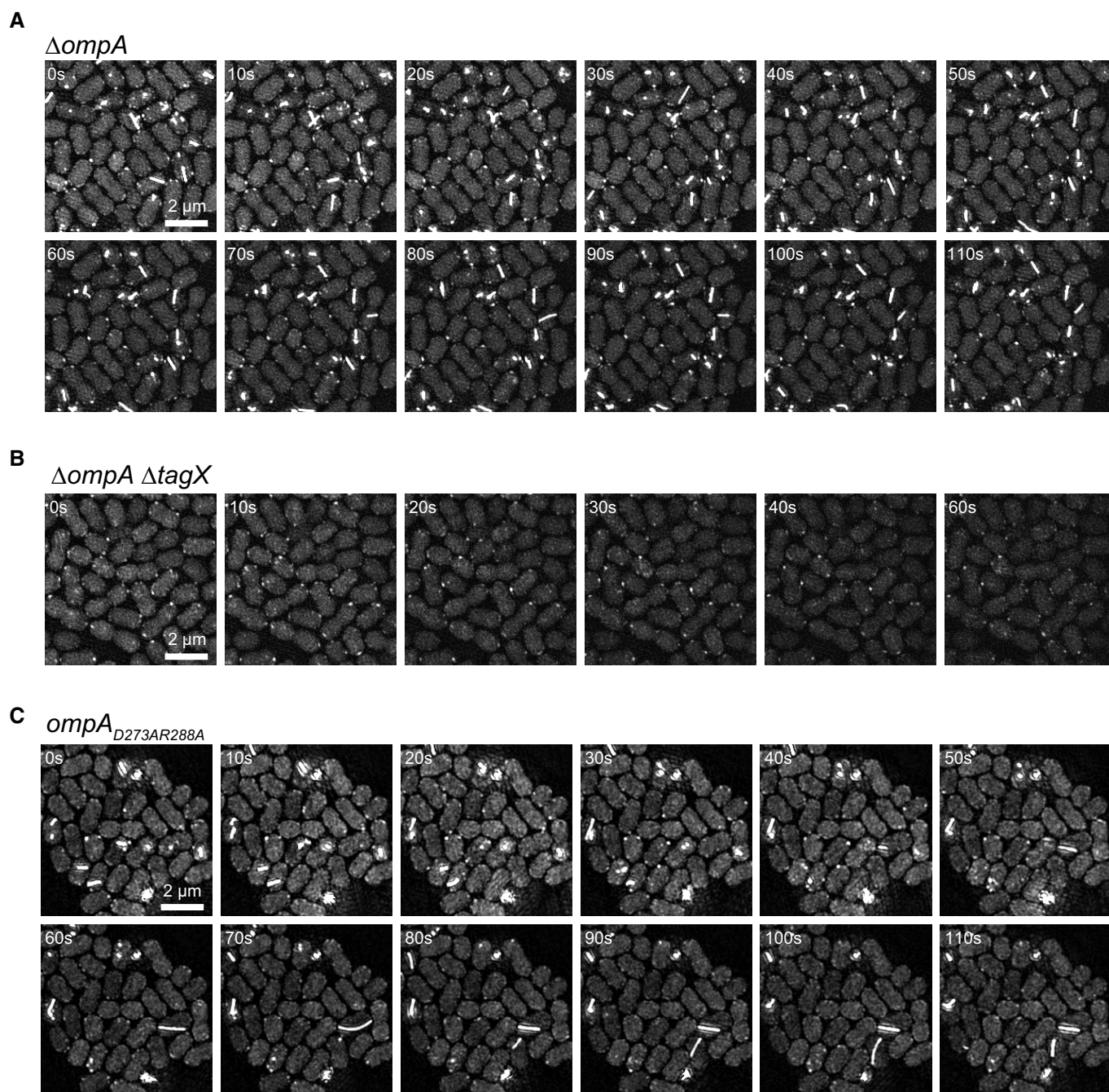


Figure 4. Lack of outer membrane OmpA leads to reduction in both overall T6SS assembly as well as the contact-dependent T6SS assembly in *A. baylyi*.

A Time-lapse 3D-SIM imaging of sheath dynamics (TssB-sfGFP) in the absence of OmpA. Larger field of view is shown as the second field of Movie EV9, left panel.

B Time-lapse 3D-SIM imaging of sheath dynamics (TssB-sfGFP) in *ompA*- and *tagX*-negative *A. baylyi* strain.

C Time-lapse 3D-SIM imaging of sheath dynamics (TssB-sfGFP) in cells where *OmpA*_{D273AR288A} was expressed.

Data information: Scale bars and time intervals are indicated.

identity with TslA in *A. baylyi* (Appendix Fig S1A). This contrasts with other structural T6SS components such as TssB and TssM that are 87% and 84% identical, respectively. To test if *A. baumannii* pre-assembles sheath foci at sites of cell–cell contact, we replaced the native copy of TssB with TssB-msfGFP fusion in two strains of

A. baumannii, DSM30011 and A118, and monitored sheath dynamics using 3D-SIM. We observed significant gaps between the cells, possibly due to capsule production. To enhance cell–cell contact, the sample was incubated at room temperature for at least 30 min to enable growth of a microcolony. The analysis of TssB-msfGFP

localization showed that both DSM30011 and A118 strains assembled sheath foci at the cell periphery as well as at cell–cell contact sites. In dense populations, $60.05 \pm 6.50\%$ and $51.17 \pm 5.16\%$ of sheath assembly were at the cell–cell contact site in DSM30011 and A118, respectively (three biological replicates, Figs 5A and EV5B, and Appendix Fig S1B, and Movie EV10). Moreover, the deletion of *tslA* in both strains led to a significant reduction in the frequency of contact-dependent assembly ($7.47 \pm 1.56\%$ for *AtsLA* in *A. baumannii* DSM30011 and $6.64 \pm 1.71\%$ for *ΔtslA* in *A. baumannii* A118; three biological replicates) (Figs 5B and EV5C, and Appendix Fig S1B). The ectopic expression of TslA restored the frequency of contact-dependent assembly to the level observed in the parental strains ($55.62 \pm 2.38\%$ for *A. baumannii* DSM30011 and $54.90 \pm 3.20\%$ for *A. baumannii* A118; three biological replicates) (Fig EV5A and D, and Appendix Fig S1B). Together, this indicates that contact-dependent initiation of T6SS assembly is conserved in *Acinetobacter* genus despite diversity in TslA sequences.

Identification of contact-dependent assembly in *Burkholderia thailandensis*

We searched for distantly related TslA-like proteins beyond the *Acinetobacter* genus. Analysis of TslA by HHPred (Hildebrand et al, 2009; Zimmermann et al, 2018) suggested a potential presence of a tetratricopeptide repeat-like (TPR) domain (Appendix Table S1). In addition, Phyre2 (Kelley et al, 2015) predicted that TslA contains several α -helices and a largely disordered C-terminal region (Appendix Fig S1C). Moreover, TslA has an isoelectric point (pI) higher than 9.5 (Appendix Table S2). We searched for potential TslA-like proteins in other T6SS clusters using the following criteria: (i) encoded upstream of *tssBC* and transcribed in the same direction; (ii) predicted to contain N-terminal signal peptide or be a putative lipoprotein; (iii) contain a TPR domain; and (iv) computed to have a high pI (> 8.7). We identified 231 of 281 type i4b T6SSs that fulfilled three of these four criteria in the SecRet6 database (Li et al, 2015) and thus potentially encoding a TslA-like protein, including the TagM1 (BTH_I2965) from the *B. thailandensis* T6SS-1 gene cluster (Appendix Fig S2, and Appendix Tables S2 and S3).

To be able to test whether *B. thailandensis* TagM1 functions similarly to TslA in *Acinetobacter*, we first generated chromosomal fusion of *tssB1* to *msfGFP*. We observed no significant difference in killing of *E. coli* prey cells by *B. thailandensis* TssB1-*msfGFP* fusion strain compared to the parental strain, suggesting that the TssB1-*msfGFP* is fully functional (Fig EV6A). Then, we followed the dynamics of *B. thailandensis* T6SS-1 using live-cell SIM imaging (Fig 5C and Movie EV11). We used both widefield fluorescence microscopy and 3D-SIM to visualize the sheath dynamics. Unfortunately, 3D-SIM caused significant bleaching and phototoxicity and therefore only short-term imaging was possible in the SIM mode. Therefore, for the analysis of sheath dynamics, we used widefield fluorescence imaging (Fig EV6B). T6SS-1 sheaths assembled on average in about 25 ± 5 s and were disassembled upon contraction over a timeframe of 22 ± 5 s ($n = 83$). Notably, nearly half of the analyzed cells had no sheath assembly during the entire imaging period (150 s). For cells that showed active assembly within the 150 s period, the overall frequency of full-length T6SS sheath assembly was 0.62 ± 0.32 assemblies per cell per min ($n = 1150$).

Importantly, we observed sheath foci pairs forming at cell–cell contact sites using 3D-SIM (453 sheath foci pairs in a total of 4583 cells). From these foci, occasionally the full-length T6SS sheath assembly was initiated (Fig 5C). Even though the overall assembly frequency is low, 3D-SIM revealed that $53.52 \pm 11.15\%$ of the total sheath assemblies are initiated from cell–cell contact site in dense populations (three biological replicates).

Importantly, in the absence of TslA-like protein homolog TagM1, T6SS assembly was almost abolished and killing of *E. coli* prey cells was undetectable (Fig EV6C). Moreover, in the absence of TagM1, small sheath foci were still present at the cell periphery, however, only two contact-dependent foci pairs were detected in 3428 cells (Fig 5D). The ectopically expressed *tagM1* from a neutral site on the chromosome under *P_{Sl2}* promoter could restore the WT-level T6SS activity (0.63 ± 0.31 assemblies per cell per min for T6SS-active cells, $n = 1452$) (Fig EV6B). In addition, ectopic expression also restored formation of T6SS sheath foci pairs at cell–cell contact sites (655 sheath foci pairs in 3,541 cells) (Fig EV6D).

Overall, this suggests that T6SS-1 of *B. thailandensis* assembles in response to cell–cell contact in a TagM1-dependent manner. This also indicates that the mechanism of contact-dependent regulation of T6SS assembly mediated by TslA-like proteins is conserved across several Gram-negative bacterial species.

Discussion

Here, we have used high-speed super-resolution imaging of T6SS to reveal the formation of small sheath foci, previously undetected by standard widefield imaging techniques (Ringel et al, 2017). We speculate that these sheath foci likely represent a few sheath rings that are assembled on a functional baseplate connected to the membrane complex. We showed that the foci colocalize with TssA and can extend to full-length sheaths with the help of TssA at the distal end of the sheath. Interestingly, while formation of these sheath foci is independent of TagX, initiation of polymerization of full-length sheaths requires TagX. Importantly, high-resolution imaging of dynamic sheaths indicates that about one third of T6SS assemblies in *A. baylyi* ADP1 are localized very precisely to the site of contact between neighboring cells (Fig 6A). It is unclear why *A. baylyi* cells have two modes of assembly that might undergo distinct regulation; however, it is possible that cells may switch between those two modes in response to different environmental signals.

It is surprising that the sheath foci often stay for an extended period of time without further polymerization into the full-length sheath. The mechanism underlying this delayed polymerization and its role is unclear. In *V. cholerae* and *E. coli*, a TssA protein is required for sheath polymerization (Santin et al, 2018; Schneider et al, 2019) and as we show here, TssA is also required for polymerization of sheaths in *A. baylyi*. Interestingly, stable sheath foci can colocalize with TssA, suggesting that the absence of TssA is unlikely to be the reason for delayed polymerization. In *V. cholerae*, TagA over-expression was shown to prevent sheath assembly (Schneider et al, 2019), however, TagA is absent in *A. baylyi*. This delay in sheath polymerization points to a regulatory mechanism, which could be common among different T6SS clusters as the small sheath foci are difficult to detect without using SIM and thus could have been previously undetected. Indeed, we show that similar sheath

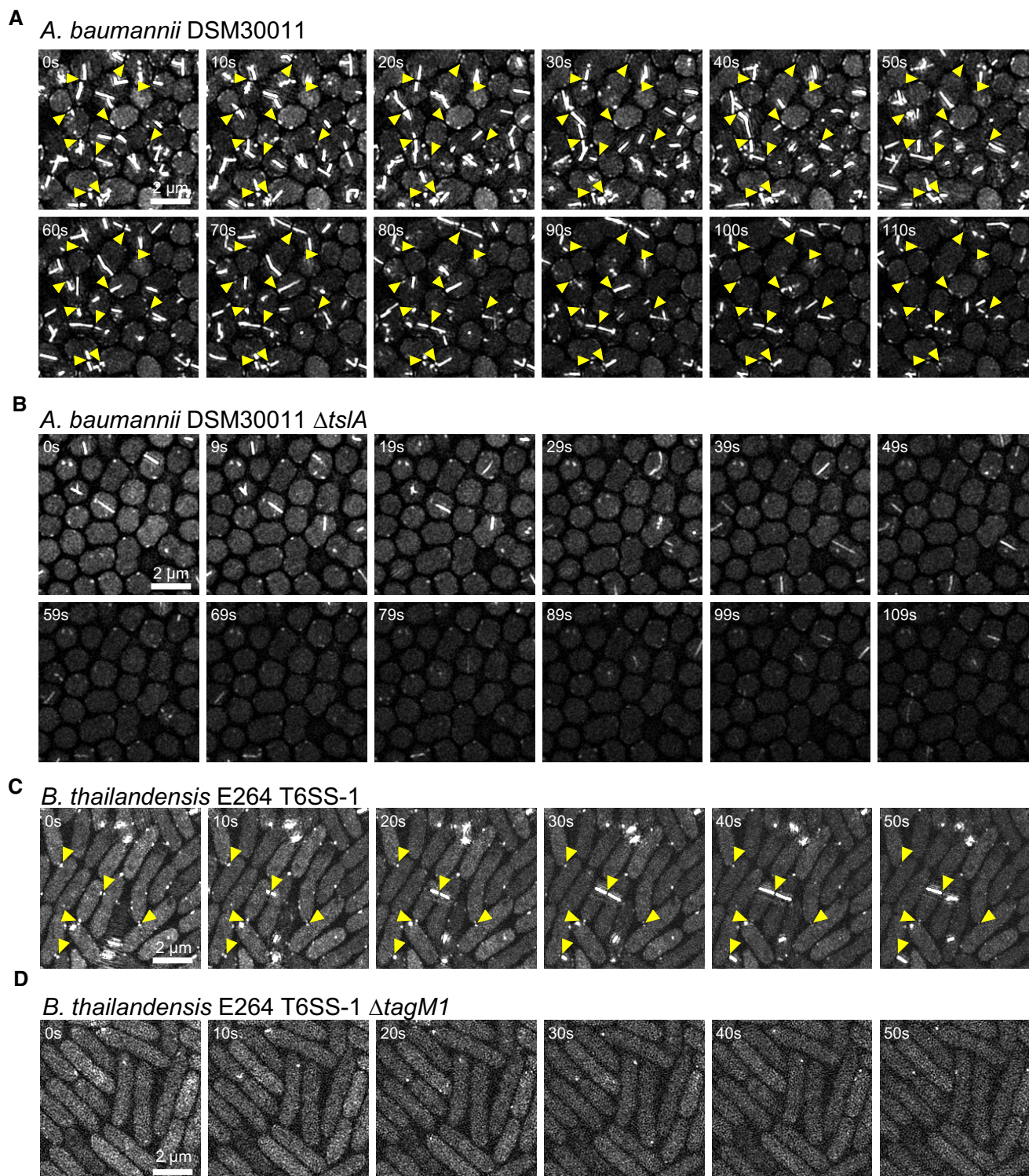


Figure 5. Contact-dependent T6SS assembly in *A. baumannii* and *B. thailandensis*.

A Time-lapse 3D-SIM imaging of T6SS assembly, contraction, and disassembly by visualizing TssB-sfGFP in cells of *A. baumannii* DSM30011.

B Time-lapse 3D-SIM imaging of sheath dynamics (TssB-sfGFP) in the absence of TslA in *A. baumannii* DSM30011.

C Time-lapse 3D-SIM imaging of sheath dynamics (TssB1-sfGFP) of *B. thailandensis* E264.

D Time-lapse 3D-SIM imaging of sheath dynamics (TssB1-sfGFP) of *B. thailandensis* E264 in the absence of *tagM1*.

Data information: Yellow arrows indicate examples of contact-dependent sheath foci or paired sheath assemblies. Larger fields of view are shown as the first field of view of Movie EV10 for *A. baumannii* and Movie EV11 for *B. thailandensis*, respectively. Scale bars and time intervals are indicated.

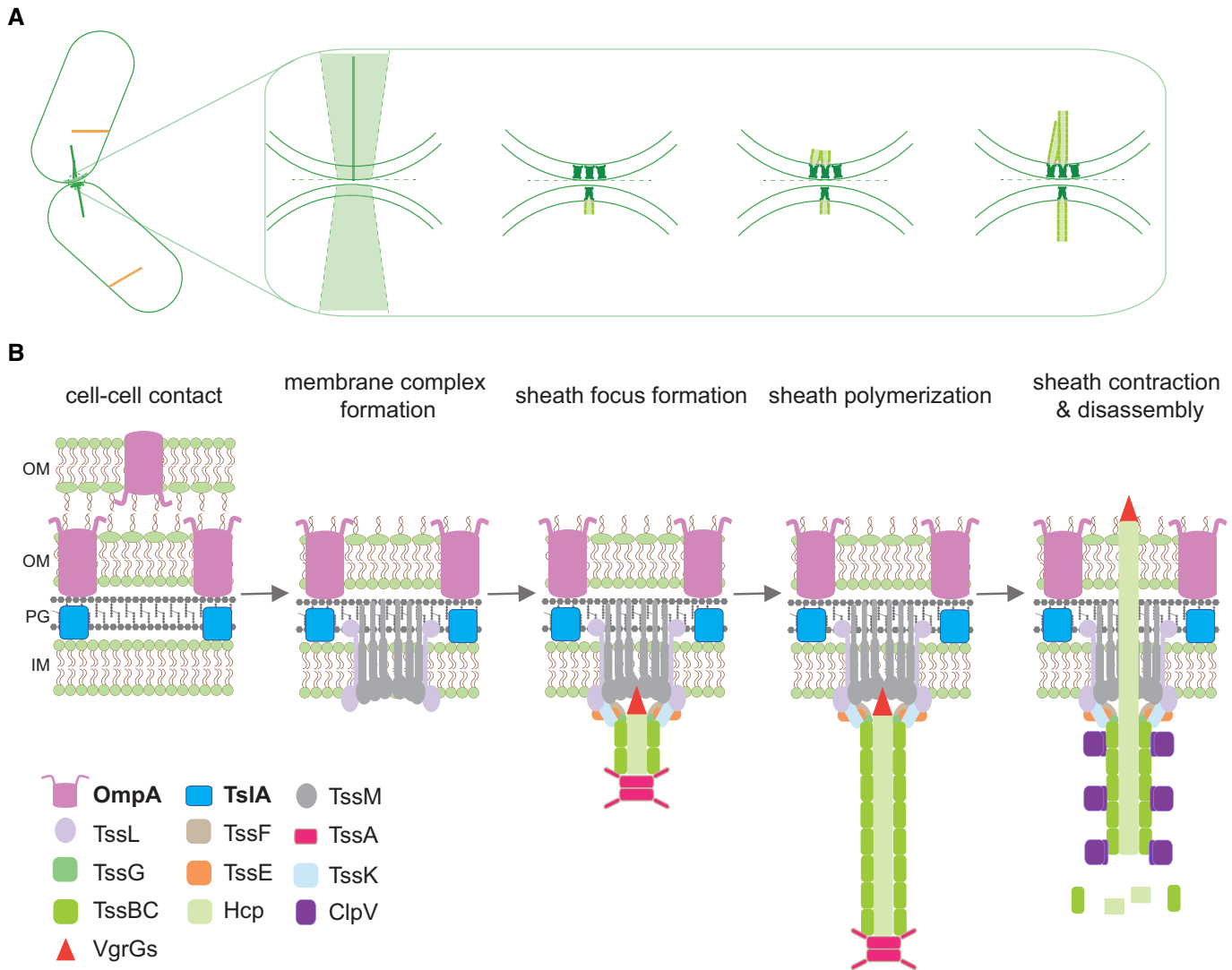


Figure 6. Proposed model of contact-dependent T6SS assembly.

A In *Acinetobacter* and *B. thailandensis*, cells in close contact with other cells can initiate membrane complex formation followed by assembly of a few rings of T6SS sheath at the site of contact, which later may continue to assembly of a full-length sheath. Several membrane complexes may form at the same contact site, which can lead to multiple sheath assemblies at the same time.

B Cells sense contact with proximal cells through a cascade dependent on the presence of TssA and OmpA. Possible interaction of TssA with TssM triggers membrane complex/baseplate assembly followed by the formation of a few sheath rings. TssA caps such sheath foci for further polymerization upon unknown signal. The Hcp tube and VgrG spike along with effectors are propelled out of the cell during sheath contraction. The ATPase ClpV then disassembles the contracted sheath.

foci are present during formation of the *B. thailandensis* T6SS-1, where the delay of full-length assembly is even more pronounced. Somewhat surprisingly, stable sheath foci formed also in the absence of TagX, which was suggested to cleave peptidoglycan to allow T6SS assembly in *A. baylyi* (Weber *et al.*, 2016). In *E. coli*, lytic transglycosylase MltE is required for membrane complex assembly and thus T6SS function (Santin & Cascales, 2017). It remains unclear how can TagX be specifically required for initiation of sheath polymerization while being dispensable for formation of the sheath foci, which require formation of the membrane complex and baseplate.

Recently, another class of proteins interacting with TssA and baseplate was identified. It was shown that TagB1 from *Pseudomonas putida* was recruited to baseplate by the TssA1 and stabilized sheath polymerization (Bernal *et al.*, 2021). Moreover, *P. putida* T6SS-1 sheaths contracted immediately after full-length assembly (Bernal *et al.*, 2021). Interestingly, T6SS sheaths in *A. baylyi* also contract immediately after assembly; however, the T6SS cluster of *A. baylyi* lacks TagB1 homolog.

Interestingly, in contrast to the assembly of H1-T6SS in *P. aeruginosa* shown to be triggered by membrane damage (Basler *et al.*, 2013; Ho *et al.*, 2013; Stolle *et al.*, 2021), T6SS assembly in *A. baylyi*

is clearly independent of T6SS attacks from neighboring cells. First, stable sheath foci pairs at cell–cell contact sites are formed in *AtagX* mutant cells, where the assembly of the functional T6SS is almost completely abolished. Second, sheath foci form at the contact site with *E. coli* cells that are unable to trigger assembly of H1-T6SS in *P. aeruginosa* (Ho *et al*, 2013). Therefore, we propose that a subset of T6SS assembly in *Acinetobacter* is triggered by a close physical contact between the membranes of neighboring cells. Indeed, we observed that the cells of the capsulated *A. baylyi* BD4 strain that were about 220 nm apart from each other lacked contact-dependent T6SS assembly.

Importantly, our data show that TslA protein is required for positioning T6SS assembly to the cell–cell contact site. Bioinformatic analysis and immunofluorescence-based localization suggest that TslA is a periplasmic protein that contains several alpha helices with a large disordered C-terminal region. Interestingly, we identified TslA-like proteins exclusively in about 80% of subtype i4b T6SS clusters (Barret *et al*, 2011, 2013; Russell *et al*, 2014b; Li *et al*, 2015). T6SS clusters encoding TslA-like protein were found in bacteria including *Acinetobacter* and *Burkholderia* species, *Achromobacter xylosoxidans*, and *Ralstonia solanacearum* (Appendix Fig S2 and Appendix Table S3). Indeed, we show that localization of *B. thailandensis* T6SS-1 to the cell–cell contact sites is dependent on TslA-like protein TagM1 (Fig 5C and D). This suggests that precise T6SS aiming in response to cell contact is widespread among bacteria with subtype i4b-T6SS. Interestingly, previous studies indicated that TslA homolog in *A. baumannii* interacts with TssM (Li *et al*, 2019). This would suggest that TslA either recruits TssM to the site of contact with neighboring cells or initiates TssM oligomerization (Fig 6B).

Here, we show that the outer membrane protein OmpA is required for localized T6SS assembly. Since the BamB/C/E components of BAM complex are dispensable for contact-dependent T6SS assembly, we suggest that OmpA is specifically required for T6SS positioning. In *Acinetobacter*, OmpA has been shown to play various functions, including formation of biofilm on abiotic surface and adhesion to host cells (Gaddy *et al*, 2009; Nie *et al*, 2020). In addition, OmpA on the surface of outer membrane vesicles (OMVs) is important for the pathogenesis of *A. baumannii* because it induces fragmentation of mitochondria in mammalian cells (Tiku *et al*, 2021). OmpA is surface exposed and thus could be involved in the recognition of surface contact (Freudl *et al*, 1986; Confer & Ayalew, 2013). Indeed, the involvement of OmpA in the recognition of neighboring cell surface has been demonstrated for F plasmid conjugation, where the outer membrane TraN interacts with OmpA on the surface of the recipient cell for mating pair stabilization (MPS) before conjugation pore forms (Klimke *et al*, 2005). Similarly, it is possible that OmpA could sense cell–cell contact in *A. baylyi* and signal this to TslA and thus initiate membrane complex assembly by TslA–TssM interaction.

The unique assembly and mode of action of T6SS allow for physical puncturing of the target cell membrane and delivery of large hydrophilic proteins across membranes of both bacterial and eukaryotic cells (Shneider *et al*, 2013; Diniz & Coulthurst, 2015). However, T6SS assembly is also apparently costly as it requires assembly, refolding, and synthesis of hundreds of proteins to deliver just a few effector proteins. During general interbacterial competition, random assembly of T6SS seems wasteful, since T6SS toxins require direct delivery to a neighboring cell. Cells that assemble their T6SS

randomly, fire their T6SS in all possible directions, and thus may miss target cells in specific locations. *P. aeruginosa* has evolved a mechanism to reduce the cost and increase efficiency of its T6SS attack by sensing when and where an attack is being initiated from (Basler *et al*, 2013). This allows *P. aeruginosa* to have all the components ready in the cytosol and assemble the T6SS quickly and directly toward the attacker (Smith *et al*, 2020). However, this mechanism requires that *P. aeruginosa* is able to withstand the initial attack and only then fire its own H1-T6SS. On the other hand, the mechanism that we describe here in *A. baylyi*, *A. baumannii*, and *B. thailandensis* allows the bacteria to directly sense where the neighboring cells are and to attack any prey cell with high precision. Such targeted firing of T6SS increases overall efficiency and speed of effector delivery into target cells and thus gives the attacking cells an advantage during competition with other bacteria. It is possible that certain bacteria could make this mechanism even more efficient by specifically recognizing prey cells and thus reduce futile firing at sister cells.

It remains to be tested what is the minimal distance between surfaces of neighboring cells or how large such contact needs to be to trigger contact-dependent T6SS assembly described here. We usually detected only a single T6SS assembly at the cell–cell contact site and only occasionally multiple assemblies were observed, however, it is important to realize that the number of T6SS assemblies could be limited within the cell, as the copy number of several T6SS components is low (Lin *et al*, 2019). Therefore, it is possible that while the surface of a cell–cell contact could accommodate multiple T6SS assemblies, this is in fact limited due to lack of certain T6SS building blocks. However, we cannot exclude that additional mechanisms play a role in limiting T6SS assembly at the contact site.

We expect that high-resolution localization of T6SS assembly in other bacteria under various conditions may unravel additional intricate mechanisms of T6SS targeting. Indeed, recent advances in live cell imaging revealed that bacteria spatially and temporally regulate subcellular localization of a variety of molecules, however, most studies have been focused on defined regions, such as a mid-cell, a polar region, or regions associated with a nucleoid (Goehring & Beckwith, 2005; Rudner & Losick, 2010; Gahlmann & Moerner, 2014; Laloux & Jacobs-Wagner, 2014). In this work, we reveal a mechanism of localization of a complex nanomachine in response to contact with another cell. Such precise positioning likely requires temporal and spatial coordination of many regulatory proteins at the membrane. Since many T6SS accessory proteins remain uncharacterized, we propose that some of these proteins might be required for spatiotemporal regulation of T6SS assembly. We expect that additional mechanisms of dynamic localization of T6SS will be identified in more bacteria and shown to play an important role in their pathogenesis or ecology.

Materials and Methods

Strains and growth conditions

A list of strains used in this work can be found in Appendix Table S4. Cells of *A. baylyi*, *A. baumannii*, *B. thailandensis*, and *E. coli* were grown in Luria–Bertani (LB) media or on LB plate containing 1.3–1.5% agar at 30 or 37°C unless stated

otherwise. Antibiotic concentrations used were ampicillin (300 µg/ml), streptomycin (50 µg/ml for liquid and 100 µg/ml for plate), kanamycin (50 µg/ml), trimethoprim (200 µg/ml), chloramphenicol (15 µg/ml), and gentamicin (15–30 µg/ml). Detailed information on the full list of strains used is available in Appendix Table S4. List of oligonucleotides used is available in Appendix Table S5.

Construction of *A. baylyi*, *A. baumannii*, and *B. thailandensis* mutants

Chromosomal mutants of *A. baylyi* were constructed as described (Metzgar et al, 2004; Ringel et al, 2017). The homologous regions used were typically 500–600 bp in length. A strain ectopically expressing *tslA* or *ompA* was constructed by fusing their own native promoters with the gene nucleotide sequence and terminators followed by the *Kan^R* gene. This sequence was then fused with the flanking region of *ampC* for integration into the *ampC* locus (between 3,515,085 bp and 3,516,109 bp).

Chromosomal mutants of *A. baumannii* DSM30011 and A118 were constructed using allelic exchange with suicide vector pGP704Sac-kan as described (Metzger et al, 2019; Vesel & Blokesch, 2021). The homologous flanking regions were between 500 and 900 bp. For conjugation, the donor *E. coli* S17-1 λpir containing pGP704Sac-kan with desired flanking regions was inserted and *A. baumannii* recipient cells were mixed at high density followed by incubation at 37°C on LB agar plates for 6 h. The cell mixture was then resuspended in LB and selected on LB agar containing chloramphenicol (15 µg/ml) and kanamycin (50 µg/ml) with overnight incubation at 37°C. Next, for the selection of second recombination events, the recombinant colonies were restreaked on LB agar plates without salt and supplemented with 10% sucrose and incubated at room temperature overnight. The desired mutation was verified by colony PCR and sequencing. Strains ectopically expressing *tslA* were constructed by replacing the AraC-inducible system with the native promoter of *tslA* followed by the *tslA* nucleotide sequence on the Tn7-based integration vector pGP704-TnAraC (Adams et al, 2019; Stutzmann & Blokesch, 2020). The integration of such vectors into *A. baumannii* chromosome was achieved by triparental mating mediated by *E. coli* S17-1 λpir with helper plasmid pUX-BF-13 (Bao et al, 1991) and selected on LB agar containing chloramphenicol (15 µg/ml) and gentamicin (15 µg/ml) with overnight incubation at 37°C.

Burkholderia thailandensis mutants were generated by allelic exchange using the suicide vector, pDONRPEX18Tp-SceI-pheS (Fazli et al, 2015). The homologous flanking regions were between 700 and 1,200 bp. For conjugation, the donor *E. coli* SM10 containing pDONRPEX18Tp-SceI-pheS with desired flanking regions inserted and *B. thailandensis* recipient cells were mixed at high density followed by incubation at 37°C on no-salt LB agar plates for 5 h. The cell mixture was then resuspended in LB and selected on LB agar containing gentamicin (30 µg/ml) and trimethoprim (200 µg/ml) with overnight incubation at 37°C. Integration of plasmid at the desired location was confirmed by colony PCR. Next, for the selection of second recombination events, the recombinant colonies were regrown on M9 agar plates supplemented with 0.4% glucose and 0.1% chloro-phenylalanine followed by a 2-day incubation at 37°C and two additional rounds of passage on such plates. The desired mutation was verified by colony PCR and sequencing.

Strains ectopically expressing *tagM1* were constructed by inserting *tagM1* nucleotide sequence fused to *P_{S12}* promoter (the *Burkholderia pseudomallei* *rpsL* promoter) (Yu & Tsang, 2006) into the Tn7-based integration vector pUC18T-mini-Tn7-Tp originated from pUC18T-mini-Tn7T; The integration of such vectors into *B. thailandensis* chromosome was achieved by triparental mating mediated by *E. coli* SM10 with helper plasmid pTNS2 (Choi et al, 2005). Cells were selected on LB agar containing gentamicin (30 µg/ml) and trimethoprim (200 µg/ml) with overnight incubation at 37°C.

Bacterial interaction assay between *B. thailandensis* and *E. coli*

For investigating if the fusion of *msfGFP* to *TssB* has effect on its T6SS function, we performed the β-galactosidase detection-based assay using the conversion of color of cell impermeable substrate chlorophenol red-β-D-galactopyranoside (CPRG) as readout as previously described (Vettiger & Basler, 2016). *B. thailandensis* cells and *E. coli* prey cells were grown in LB to reach an OD₆₀₀ of ~ 1. Both prey and predator strains were harvested and concentrated to an OD₆₀₀ of 10 and mixed in ratio of 10:1. For each mixture, 5 µl was spotted on LB agar containing 20 µg/ml CPRG and 100 µM isopropyl-β-D-thiogalactopyranoside (IPTG) and incubated at 37°C for 3 h.

For following the lysis dynamics of the CPRG-based competition assay, *B. thailandensis* cells were grown to reach an OD₆₀₀ of ~ 1. The *E. coli* prey cells were grown in LB containing 100 µM IPTG to pre-induce the production of β-galactosidase. Both prey and predator strains were harvested and concentrated to an OD₆₀₀ of 10 and mixed in ratios as indicated. For each mixture, 3 µl was spotted on LB agar containing 20 µg/ml CPRG and 100 µM IPTG in a flat-bottom 96-well plate. The plate was then incubated at 30°C without a lid in a Synergy H1M2 plate reader (BioTEK) for 10 h, while measuring absorbance at 572 nm every 10 min.

Immunofluorescence

Acinetobacter baylyi cells were grown in LB to OD₆₀₀ of 1.0 to 1.5. Cells were then fixed with 2% paraformaldehyde in wells on immunofluorescence slides (Polysciences) for 25 min, whose slide wells were pre-incubated with 0.01% (v/v) poly-L-lysine (Sigma Aldrich) for at least 1 h at room temperature followed by washing with water and removal of excess liquid. The attached cells were then washed three times with PBS followed by 20 min incubation in Glucose–Tris–EDTA buffer. For localization of *TslA* in the absence of signal peptide, the attached cells were additionally incubated in Glucose–Tris–EDTA buffer containing 0.1–0.5% Triton X-100. Cells were then blocked with PBS containing 3% BSA for another 20 min. Staining was performed using a polyclonal rabbit antibody against *TslA* (generated by GenScript, diluted 1:50) followed by secondary antibody Goat anti-Rabbit IgG (H + L) Alexa Fluor Plus 594 (diluted 1:400). SlowFade Diamond Antifade Mountant (Thermo Fisher) was applied before imaging. Bacterial cells were imaged using widefield microscope as described below.

Widefield microscopy

The Nikon Ti-E inverted microscope equipped with Perfect Focus System and Plan Apo 100x Oil Ph3 DM (NA 1.4) objective lens,

SPECTRA X light engine (Lumencor), along with ET-GFP (Chroma #49002) and ET-mCherry (Chroma #49008) filter set for fluorescence excitation, and filtration was used in this work. sCMOS camera pco.edge 4.2 with pixel size of 65 nm (PCO) and VisiView software (Visitron Systems) were used for imaging. Imaging was set at 30°C with 95% humidity controlled by Okolab T-unit (Okolab). Image analysis was conducted in Fiji (Schindelin *et al*, 2012) and customized plugin based on StackReg 3D (Thevenaz *et al*, 1998; Ringel *et al*, 2017).

Western blotting

For detection of OmpA, *A. baylyi* cells were grown in LB and adjusted to OD₆₀₀ of 1 in SDS loading buffer. Proteins from lysed cells were separated on Mini-PROTEAN[®] Precast Gels (Bio-Rad) and transferred to nitrocellulose membrane for immune detection. Primary antibody against OmpA (generated by Genscript) was added at concentration of 0.25 µg/ml in PBS buffer with 5% milk containing 0.1% Tween 20 (PBST). Membrane was incubated for 1.5 h, followed by another 1.5 h incubation with PBST containing horseradish peroxidase-labeled anti-rabbit antibody (Jackson Lab). Peroxidase-labeled conjugates were detected by LumiGLO Chemiluminescent Substrate (Seracare) on a Gel Imager (GE ImageQuant LAS 4000).

Structured illumination microscopy (SIM)

Acinetobacter baylyi or *A. baumannii* cells were grown on a LB agar plate at 30°C overnight; cells from about 0.5 cm² were restreaked and grown on a fresh LB agar plate at 37°C for 1.5–2 h. Cells were then removed from the plate and resuspended in 30–50 µl of LB medium to obtain high-density cell suspension (OD₆₀₀ 10–30). The cell suspension was spotted onto a thin pad containing 1% agarose in LB:PBS (1:2 ratio) mixture and covered with a coverslip. For imaging of *A. baumannii*, the sample was additionally incubated at room temperature for at least 30 min right before imaging to achieve close cell–cell contact without accumulation of contracted (but not disassembled) sheaths. For imaging of co-incubation of *A. baylyi* and *E. coli*, both species were mixed in 1:1 ratio when resuspending separate overnight cultures but otherwise grown and prepared for imaging as described above for *A. baylyi*. *B. thailandensis* cells were cultivated at 37°C in LB. After overnight cultivation, cells were diluted in LB and grown for 3–4 h to an OD_{600nm} of 0.8–1.2 before concentrating to high density (OD₆₀₀ 10–20) in LB. Cell suspensions were then spotted onto a thin pad containing 1% agarose in LB:PBS (1:2 ratio) mixture and covered with a coverslip.

Image acquisition was performed using a DeltaVision OMX Blaze (GE Healthcare) or OMX Flex (Cytiva) equipped with UltimateFocus Hardware Autofocus module with Focus Assist and sCMOS cameras. The 60×/1.42 NA Plan Apo N objective (Olympus) was used. The 488 and 568 nm excitation lasers were used. For time-lapse analysis, acquisition was performed with 5 or 10 s intervals for at least 1 min. Immersion oil with refractive index 1.516 was used. For TssB-sfGFP, a 488 nm laser power of 5–10% with 5–10 ms exposure time was applied and 3D-SIM imaging was conducted. For 3D-SIM, nine z-stacks with 125 nm per step were acquired. For TssB and TssA co-imaging, 2D-SIM on OMX Flex was used; for TssB-mCherry2, a 568 nm laser power of 10% with 20 ms exposure time

was applied; and for TssA-mNeonGreen, a 488 nm laser power of 10% with 30 ms exposure time was applied. Reconstruction was performed using DeltaVision OMX softWoRx with Wiener filter value set at 0.005 (DeltaVision OMX Blaze) or 0.001 (OMX Flex). Pixel size after reconstruction is 40 nm. After reconstruction, a maximal intensity projection through z was calculated and shown for 3D-SIM. Quantification of T6SS sheath assembly speed in *A. baylyi* was conducted in Fiji on time-lapse series using 3D-SIM (every 5 s for 3–5 min). A total of 300 T6SS structures were analyzed. Quantification of T6SS dynamic cycles was conducted in Fiji on time-lapse series using 3D-SIM (every 5 s for 3–5 min). A total of 63 T6SS structures with full cycle of polymerization, contraction, and complete disassembly were analyzed. For quantification of frequency of contact-dependent T6SS in *A. baylyi* and *A. baumannii*, assemblies over the period of time-lapse series for 2–3 min acquired by 3D-SIM were counted as either contact dependent or contact independent. Fig 1B illustrated the criteria used for quantification to differentiate between contact-dependent and contact-independent T6SS assembly. At least 500 cells were analyzed for each replicate. Three biological replicates were analyzed for each strain. Statistical analysis was performed using unpaired *t*-test in Prism GraphPad 8. Quantification of T6SS sheath assembly speed in *B. thailandensis* was performed on time-lapse series (every 5 s for 2.5 min) acquired by widefield microscopy, with 83 structures with full dynamic cycle were analyzed. Quantification of contact-dependent T6SS sheath foci pair formation in *B. thailandensis* was conducted on time-lapse series using 3D-SIM (every 5 s for 1–2 min).

Bioinformatics analysis

Secondary structure prediction of proteins was performed using the Phyre2 server (Kelley *et al*, 2015). Protein alignment was conducted using MUSCLE alignment (Edgar, 2004; Madeira *et al*, 2019) and visualized using JalView (Waterhouse *et al*, 2009). Subtype i4b T6SS clusters were obtained from SecRet6 database (Li *et al*, 2015). NCBI (NCBI Resource Coordinators, 2018), Uniprot (The UniProt Consortium, 2019), SignalP 5.1 (Almagro Armenteros *et al*, 2019), and HHpred (Söding, 2005; Hildebrand *et al*, 2009; Zimmermann *et al*, 2018) were used to obtain DNA/protein sequences and predict the presence of signal peptide, specific domains, and structural motifs. Schematic representation of gene clusters was performed using Gene Graphics web application (Harrison *et al*, 2018).

Data availability

This study includes no data deposited in external repositories.

Expanded View for this article is available online.

Acknowledgements

The work was supported by the Swiss National Science Foundation (grant BSSG10_155778), European Research Council consolidator grant (865105 - “AimingT6SS”), and the University of Basel. The authors thank all members of the Basler lab for excellent assistance and helpful discussions. We also thank the Imaging Core Facility of Biozentrum, University of Basel, for their great help. We thank Prof. Gan Yunn Hwen (NUS) for sharing the wild-type

B. thailandensis E264 strain, and Prof. Melanie Blokesch (EPFL) and Prof. Urs Jenal (University of Basel) for kindly sharing plasmids. Open access funding provided by Universitat Basel.

Author contributions

Lin Lin: Conceptualization; Resources; Data curation; Formal analysis; Validation; Investigation; Visualization; Methodology; Writing—original draft; Writing—review & editing. **Raffaella Capozzoli:** Conceptualization; Data curation; Formal analysis; Investigation; Visualization; Methodology; Writing—original draft. **Alexia Ferrand:** Data curation; Formal analysis; Validation; Investigation; Methodology. **Miro Plum:** Supervision; Validation; Investigation; Methodology. **Andrea Vettiger:** Validation; Investigation; Methodology. **Marek Basler:** Conceptualization; Data curation; Supervision; Funding acquisition; Validation; Investigation; Methodology; Writing—original draft; Project administration; Writing—review & editing.

In addition to the CRediT author contributions listed above, the contributions in detail are:

LL and MB designed the experiments; LL and RC performed the mutagenesis and live imaging experiments as well as statistical analysis; AF and AV contributed to initial acquisition of SIM data and method development; MP contributed to initial method development of mutagenesis in *B. thailandensis*; LL analyzed the SIM imaging data; and LL and MB wrote the manuscript.

Disclosure and competing interests statement

The authors declare that they have no conflict of interest.

References

- Adams DW, Stutzmann S, Stoudmann C, Blokesch M (2019) DNA-uptake pili of *Vibrio cholerae* are required for chitin colonization and capable of kin recognition via sequence-specific self-interaction. *Nat Microbiol* 4: 1545–1557
- Almagro Armenteros JJ, Tsirigos KD, Sønderby CK, Petersen TN, Winther O, Brunak S, von Heijne G, Nielsen H (2019) SignalP 5.0 improves signal peptide predictions using deep neural networks. *Nat Biotechnol* 37: 420–423
- Aoki SK, Pamma R, Hernday AD, Bickham JE, Braaten BA, Low DA (2005) Contact-dependent inhibition of growth in *Escherichia coli*. *Science* 309: 1245–1248
- Aoki SK, Webb JS, Braaten BA, Low DA (2009) Contact-dependent growth inhibition causes reversible metabolic downregulation in *Escherichia coli*. *J Bacteriol* 191: 1777–1786
- Aschtgen M-S, Gavioli M, Dessen A, Llobès R, Cascales E (2010) The SciZ protein anchors the enteroaggregative *Escherichia coli* Type VI secretion system to the cell wall. *Mol Microbiol* 75: 886–899
- Bao Y, Lies DP, Fu H, Roberts GP (1991) An improved Tn7-based system for the single-copy insertion of cloned genes into chromosomes of gram-negative bacteria. *Gene* 109: 167–168
- Barret M, Egan F, Fargier E, Morrissey JP, O’Gara F (2011) Genomic analysis of the type VI secretion systems in *Pseudomonas* spp.: novel clusters and putative effectors uncovered. *Microbiology* 157: 1726–1739
- Barret M, Egan F, O’Gara F (2013) Distribution and diversity of bacterial secretion systems across metagenomic datasets. *Environ Microbiol Rep* 5: 117–126
- Basler M, Ho BT, Mekalanos JJ (2013) Tit-for-tat: type VI secretion system counterattack during bacterial cell-cell interactions. *Cell* 152: 884–894
- Basler M, Mekalanos JJ (2012) Type 6 secretion dynamics within and between bacterial cells. *Science* 337: 815
- Basler M, Pilhofer M, Henderson GP, Jensen GJ, Mekalanos JJ (2012) Type VI secretion requires a dynamic contractile phage tail-like structure. *Nature* 483: 182–186
- Bernal P, Furniss RCD, Fecht S, Leung RCY, Spiga L, Mavridou DA, Filloux A (2021) A novel stabilization mechanism for the type VI secretion system sheath. *Proc Natl Acad Sci U S A* 118: e2008500118
- Bingle LE, Bailey CM, Pallen MJ (2008) Type VI secretion: a beginner’s guide. *Curr Opin Microbiol* 11: 3–8
- Bönemann G, Pietrosiuk A, Diemand A, Zentgraf H, Mogk A (2009) Remodelling of VipA/VipB tubules by ClpV-mediated threading is crucial for type VI protein secretion. *EMBO J* 28: 315–325
- Brodmann M, Dreier RF, Broz P, Basler M (2017) *Francisella* requires dynamic type VI secretion system and ClpB to deliver effectors for phagosomal escape. *Nat Commun* 8: 1–12
- Casabona MG, Silverman JM, Sall KM, Boyer F, Couté Y, Poirel J, Grunwald D, Mougous JD, Elsen S, Attree I (2013) An ABC transporter and an outer membrane lipoprotein participate in posttranslational activation of type VI secretion in *Pseudomonas aeruginosa*. *Environ Microbiol* 15: 471–486
- Cascales E, Buchanan SK, Duché D, Kleantous C, Llobès R, Postle K, Riley M, Slatin S, Cavard D (2007) Colicin biology. *Microbiol Mol Biol Rev* 71: 158–229
- Cherrak Y, Rapisarda C, Pellarin R, Bouvier G, Bardiaux B, Allain F, Malosse C, Rey M, Chamot-Rooke J, Cascales E et al (2018) Biogenesis and structure of a type VI secretion baseplate. *Nat Microbiol* 3: 1404–1416
- Cho S-H, Szweczyk J, Pesavento C, Zietek M, Banzhaf M, Roszczenko P, Asmar A, Laloux G, Hov A-K, Leverrier P et al (2014) Detecting envelope stress by monitoring β -barrel assembly. *Cell* 159: 1652–1664
- Choi K-H, Gaynor JB, White KG, Lopez C, Bosio CM, Karkhoff-Schweizer RR, Schweizer HP (2005) A Tn7-based broad-range bacterial cloning and expression system. *Nat Methods* 2: 443–448
- Confer AW, Ayalew S (2013) The OmpA family of proteins: roles in bacterial pathogenesis and immunity. *Vet Microbiol* 163: 207–222
- Cornforth DM, Foster KR (2013) Competition sensing: the social side of bacterial stress responses. *Nat Rev Microbiol* 11: 285–293
- Diniz JA, Coulthurst SJ (2015) Intraspecies competition in *Serratia marcescens* is mediated by type VI-secreted rhs effectors and a conserved effector-associated accessory protein. *J Bacteriol* 197: 2350–2360
- Diniz JA, Liu Y-C, Coulthurst SJ (2015) Molecular weaponry: diverse effectors delivered by the Type VI secretion system. *Cell Microbiol* 17: 1742–1751
- Durand E, Cambillau C, Cascales E, Journet L (2014) VgrG, Tae, Tle, and beyond: the versatile arsenal of Type VI secretion effectors. *Trends Microbiol* 22: 498–507
- Durand E, Nguyen VS, Zoued A, Logger L, Péhau-Arnaudet G, Aschtgen M-S, Spinelli S, Desmyter A, Bardiaux B, Dujeancourt A et al (2015) Biogenesis and structure of a type VI secretion membrane core complex. *Nature* 523: 555–560
- Durand E, Zoued A, Spinelli S, Watson PJH, Aschtgen M-S, Journet L, Cambillau C, Cascales E (2012) Structural Characterization and oligomerization of the TssL protein, a component shared by bacterial type VI and type IVb secretion systems. *J Biol Chem* 287: 14157–14168
- Edgar RC (2004) MUSCLE: multiple sequence alignment with high accuracy and high throughput. *Nucleic Acids Res* 32: 1792–1797
- Fazli M, Harrison JJ, Gambino M, Givskov M, Tolker-Nielsen T (2015) In-frame and unmarked gene deletions in *Burkholderia cenocepacia* via an allelic exchange system compatible with gateway technology. *Appl Environ Microbiol* 81: 3623–3630
- Felisberto-Rodrigues C, Durand E, Aschtgen M-S, Blangy S, Ortiz-Lombardia M, Douzi B, Cambillau C, Cascales E (2011) Towards a structural

- comprehension of bacterial type VI secretion systems: characterization of the TssJ-TssM complex of an *Escherichia coli* pathovar. *PLoS Pathog* 7: e1002386
- Filloux A, Freemont P (2016) Structural biology: baseplates in contractile machines. *Nature Microbiology* 1: 1–2
- Förster A, Planamente S, Manoli E, Lossi NS, Freemont PS, Filloux A (2014) Coevolution of the ATPase ClpV, the sheath proteins TssB and TssC, and the accessory protein TagJ/HsiE1 distinguishes type VI secretion classes. *J Biol Chem* 289: 33032–33043
- Freudl R, MacIntyre S, Degen M, Henning U (1986) Cell surface exposure of the outer membrane protein OmpA of *Escherichia coli* K-12. *J Mol Biol* 188: 491–494
- Fritsch MJ, Trunk K, Diniz JA, Guo M, Trost M, Coulthurst SJ (2013) Proteomic identification of novel secreted antibacterial toxins of the *Serratia marcescens* type VI secretion system. *Mol Cell Proteomics* 12: 2735–2749
- Gaddy JA, Tomaras AP, Actis LA (2009) The *Acinetobacter baumannii* 19606 OmpA protein plays a role in biofilm formation on abiotic surfaces and in the interaction of this pathogen with eukaryotic cells. *Infect Immun* 77: 3150–3160
- Gahlmann A, Moerner WE (2014) Exploring bacterial cell biology with single-molecule tracking and super-resolution imaging. *Nat Rev Microbiol* 12: 9–22
- Garcia EC (2018) Contact-dependent interbacterial toxins deliver a message. *Curr Opin Microbiol* 42: 40–46
- Gerc AJ, Diepold A, Trunk K, Porter M, Rickman C, Armitage JP, Stanley-Wall NR, Coulthurst SJ (2015) Visualization of the *Serratia* type VI secretion system reveals unprovoked attacks and dynamic assembly. *Cell Rep* 12: 2131–2142
- Goehring NW, Beckwith J (2005) Diverse paths to midcell: assembly of the bacterial cell division machinery. *Curr Biol* 15: R514–R526
- Hachani A, Wood TE, Filloux A (2016) Type VI secretion and anti-host effectors. *Curr Opin Microbiol* 29: 81–93
- Harrison KJ, de Crécy-Lagard V, Zallot R (2018) Gene Graphics: a genomic neighborhood data visualization web application. *Bioinformatics* 34: 1406–1408
- Heidelberger M, Das A, Juni E (1969) Immunochemistry of the capsular polysaccharide of an *Acinetobacter*. *Proc Natl Acad Sci U S A* 63: 47–50
- Heras B, Totsika M, Peters KM, Paxman JJ, Gee CL, Jarrott RJ, Perugini MA, Whitten AE, Schembri MA (2014) The antigen 43 structure reveals a molecular Velcro-like mechanism of autotransporter-mediated bacterial clumping. *Proc Natl Acad Sci U S A* 111: 457–462
- Hildebrand A, Remmert M, Biegert A, Söding J (2009) Fast and accurate automatic structure prediction with HHpred. *Proteins* 77: 128–132
- Ho BT, Basler M, Mekalanos JJ (2013) Type 6 secretion system-mediated immunity to type 4 secretion system-mediated gene transfer. *Science* 342: 250–253
- Hsu F, Schwarz S, Mougous JD (2009) TagR promotes PpkA-catalysed type VI secretion activation in *Pseudomonas aeruginosa*. *Mol Microbiol* 72: 1111–1125
- Juni E (1972) Interspecies transformation of *Acinetobacter*: genetic evidence for a ubiquitous genus. *J Bacteriol* 112: 917–931
- Juni E, Janik A (1969) Transformation of *Acinetobacter calco-aceticus* (*Bacterium anitratum*). *J Bacteriol* 98: 281–288
- Kamal F, Liang X, Manera K, Pei T-T, Kim H, Lam LG, Pun A, Hersch SJ, Dong TG (2020) Differential cellular response to translocated toxic effectors and physical penetration by the type VI secretion system. *Cell Rep* 31: 107766
- Kapitein N, Bönenmann G, Pietrosiuk A, Seyffer F, Hausser I, Locker JK, Mogk A (2013) ClpV recycles VipA/VipB tubules and prevents non-productive tubule formation to ensure efficient type VI protein secretion. *Mol Microbiol* 87: 1013–1028
- Kelley LA, Mezulis S, Yates CM, Wass MN, Sternberg MJE (2015) The Phyre2 web portal for protein modeling, prediction and analysis. *Nat Protoc* 10: 845–858
- Klebba PE, Newton SM (1998) Mechanisms of solute transport through outer membrane porins: burning down the house. *Curr Opin Microbiol* 1: 238–247
- Klimke WA, Rypien CD, Klinger B, Kennedy RA, Rodriguez-Maillard JM, Frost LSY (2005) The mating pair stabilization protein, TraN, of the F plasmid is an outer-membrane protein with two regions that are important for its function in conjugation. *Microbiology* 151: 3527–3540
- Konovalova A, Kahne DE, Silhavy TJ (2017) Outer membrane biogenesis. *Annu Rev Microbiol* 71: 539–556
- Kudryashev M, Wang RY-R, Brackmann M, Scherer S, Maier T, Baker D, DiMaio F, Stahlberg H, Egelman EH, Basler M (2015) Structure of the type VI secretion system contractile sheath. *Cell* 160: 952–962
- Laloux G, Jacobs-Wagner C (2014) How do bacteria localize proteins to the cell pole? *J Cell Sci* 127: 11–19
- Laubacher ME, Ades SE (2008) The Rcs phosphorelay is a cell envelope stress response activated by peptidoglycan stress and contributes to intrinsic antibiotic resistance. *J Bacteriol* 190: 2065–2074
- Leiman PG, Basler M, Ramagopal UA, Bonanno JB, Sauder JM, Pukatzki S, Burley SK, Almo SC, Mekalanos JJ (2009) Type VI secretion apparatus and phage tail-associated protein complexes share a common evolutionary origin. *Proc Natl Acad Sci U S A* 106: 4154–4159
- Li G-W, Burkhardt D, Gross C, Weissman JS (2014) Quantifying absolute protein synthesis rates reveals principles underlying allocation of cellular resources. *Cell* 157: 624–635
- Li J, Yao Y, Xu HH, Hao L, Deng Z, Rajakumar K, Ou H-Y (2015) SecReT6: a web-based resource for type VI secretion systems found in bacteria. *Environ Microbiol* 17: 2196–2202
- Li L, Wang Y-N, Jia H-B, Wang P, Dong J-F, Deng J, Lu F-M, Zou Q-H (2019) The type VI secretion system protein AsaA in *Acinetobacter baumannii* is a periplasmic protein physically interacting with TssM and required for T6SS assembly. *Sci Rep* 9: 9438
- Lin J-S, Pissaridou P, Wu H-H, Tsai M-D, Filloux A, Lai E-M (2018) TagF-mediated repression of bacterial type VI secretion systems involves a direct interaction with the cytoplasmic protein Fha. *J Biol Chem* 293: 8829–8842
- Lin J-S, Wu H-H, Hsu P-H, Ma L-S, Pang Y-Y, Tsai M-D, Lai E-M (2014) Fha interaction with phosphothreonine of TssL activates type VI secretion in *Agrobacterium tumefaciens*. *PLoS Pathog* 10: e1003991
- Lin L, Lezan E, Schmidt A, Basler M (2019) Abundance of bacterial Type VI secretion system components measured by targeted proteomics. *Nat Commun* 10: 1–11
- Ma L-S, Lin J-S, Lai E-M (2009) An IcmF family protein, ImpLM, is an integral inner membrane protein interacting with ImpKL, and its Walker A motif is required for type VI secretion system-mediated Hcp secretion in *Agrobacterium tumefaciens*. *J Bacteriol* 191: 4316–4329
- Ma L-S, Narberhaus F, Lai E-M (2012) IcmF family protein TssM exhibits ATPase activity and energizes type VI secretion. *J Biol Chem* 287: 15610–15621
- Madeira F, Park YM, Lee J, Buso N, Gur T, Madhusoodanan N, Basutkar P, Tivey ARN, Potter SC, Finn RD et al (2019) The EMBL-EBI search and sequence analysis tools APIs in 2019. *Nucleic Acids Res* 47: W636–W641
- Merkier AK, Centrón D (2006) bla_{OXA-51}-type β-lactamase genes are ubiquitous and vary within a strain in *Acinetobacter baumannii*. *Int J Antimicrob Agents* 28: 110–113

- Metzgar D, Bacher JM, Pezo V, Reader J, Döring V, Schimmel P, Marlière P, de Crécy-Lagard V (2004) *Acinetobacter* sp. ADP1: an ideal model organism for genetic analysis and genome engineering. *Nucleic Acids Res* 32: 5780–5790
- Metzger LC, Matthey N, Stoudmann C, Collas EJ, Blokesch M (2019) Ecological implications of gene regulation by TfoX and TfoY among diverse *Vibrio* species. *Environ Microbiol* 21: 2231–2247
- Michel-Briand Y, Baysse C (2002) The pyocins of *Pseudomonas aeruginosa*. *Biochimie* 84: 499–510
- Mougous JD, Gifford CA, Ramsdell TL, Mekalanos JJ (2007) Threonine phosphorylation post-translationally regulates protein secretion in *Pseudomonas aeruginosa*. *Nat Cell Biol* 9: 797–803
- Nazarov S, Schneider JP, Brackmann M, Goldie KN, Stahlberg H, Basler M (2018) Cryo-EM reconstruction of Type VI secretion system baseplate and sheath distal end. *EMBO J* 37: e97103
- NCBI Resource Coordinators (2018) Database resources of the National Center for Biotechnology Information. *Nucleic Acids Res* 46: D8–D13
- Nie D, Hu Y, Chen Z, Li M, Hou Z, Luo X, Mao X, Xue X (2020) Outer membrane protein A (OmpA) as a potential therapeutic target for *Acinetobacter baumannii* infection. *J Biomed Sci* 27: 26
- Ostrowski A, Cianfanelli FR, Porter M, Mariano G, Peltier J, Wong JJ, Swedlow JR, Trost M, Coulthurst SJ (2018) Killing with proficiency: integrated post-translational regulation of an offensive Type VI secretion system. *PLoS Pathog* 14: e1007230
- Park JS, Lee WC, Yeo KJ, Ryu K-S, Kumarasiri M, Hsek D, Lee M, Mobashery S, Song JH, Kim SI et al (2012) Mechanism of anchoring of OmpA protein to the cell wall peptidoglycan of the gram-negative bacterial outer membrane. *FASEB J* 26: 219–228
- Park Y-J, Lacourse KD, Cambillau C, DiMaio F, Mougous JD, Velesler D (2018) Structure of the type VI secretion system TssK–TssF–TssG baseplate subcomplex revealed by cryo-electron microscopy. *Nat Commun* 9: 1–11
- Patel RN, Mazumdar S, Ornston LN (1975) Beta-ketoadipate enol-lactone hydrolases I and II from *Acinetobacter calcoaceticus*. *J Biol Chem* 250: 6567
- Pietrosiuk A, Lenherr ED, Falk S, Bönemann G, Kopp J, Zentgraf H, Sinning I, Mogk A (2011) Molecular basis for the unique role of the AAA+ chaperone ClpV in type VI protein secretion. *J Biol Chem* 286: 30010–30021
- Pukatzki S, Ma AT, Sturtevant D, Krastins B, Sarracino D, Nelson WC, Heidelberg JF, Mekalanos JJ (2006) Identification of a conserved bacterial protein secretion system in *Vibrio cholerae* using the *Dictyostelium* host model system. *Proc Natl Acad Sci USA* 103: 1528–1533
- Pukatzki S, Ma AT, Revel AT, Sturtevant D, Mekalanos JJ (2007) Type VI secretion system translocates a phage tail spike-like protein into target cells where it cross-links actin. *Proc Natl Acad Sci USA* 104: 15508–15513
- Ramirez MS, Don M, Merquier AK, Bistué AJS, Zorreguieta A, Centrón D, Tolmasky ME (2010) Naturally competent *Acinetobacter baumannii* clinical isolate as a convenient model for genetic studies. *J Clin Microbiol* 48: 1488–1490
- Reusch RN (2012) Insights into the structure and assembly of *Escherichia coli* outer membrane protein A. *FEBS J* 279: 894–909
- Ringel PD, Hu D, Basler M (2017) The role of type VI secretion system effectors in target cell lysis and subsequent horizontal gene transfer. *Cell Rep* 21: 3927–3940
- Rudner DZ, Losick R (2010) Protein subcellular localization in bacteria. *Cold Spring Harb Perspect Biol* 2: a000307
- Russell AB, Peterson SB, Mougous JD (2014a) Type VI secretion system effectors: poisons with a purpose. *Nat Rev Microbiol* 12: 137–148
- Russell A, Wexler A, Harding B, Whitney J, Bohn A, Goo Y, Tran B, Barry N, Zheng H, Peterson S et al (2014b) A Type VI secretion-related pathway in bacteroidetes mediates interbacterial antagonism. *Cell Host Microbe* 16: 227–236
- Santin YG, Cascales E (2017) Domestication of a housekeeping transglycosylase for assembly of a Type VI secretion system. *EMBO Rep* 18: 138–149
- Santin YG, Doan T, Lebrun R, Espinosa L, Journet L, Cascales E (2018) *In vivo* TssA proximity labelling during type VI secretion biogenesis reveals TagA as a protein that stops and holds the sheath. *Nature Microbiology* 3: 1304–1313
- Schindelin J, Arganda-Carreras I, Frise E, Kaynig V, Longair M, Pietzsch T, Preibisch S, Rueden C, Saalfeld S, Schmid B et al (2012) Fiji: an open-source platform for biological-image analysis. *Nat Methods* 9: 676–682
- Schneider JP, Nazarov S, Adaixo R, Liuzzo M, Ringel PD, Stahlberg H, Basler M (2019) Diverse roles of TssA-like proteins in the assembly of bacterial type VI secretion systems. *EMBO J* 38: e100825
- Schwarz S, Singh P, Robertson JD, LeRoux M, Skerrett SJ, Goodlett DR, West TE, Mougous JD (2014) VgrG-5 Is a *Burkholderia* Type VI secretion system-exported protein required for multinucleated giant cell formation and virulence. *Infect Immun* 82: 1445–1452
- Sgro GG, Costa TRD, Cenens W, Souza DP, Cassago A, Coutinho de Oliveira L, Salinas RK, Portugal RV, Farah CS, Waksman G (2018) Cryo-EM structure of the bacteria-killing type IV secretion system core complex from *Xanthomonas citri*. *Nat Microbiol* 3: 1429–1440
- Sgro GG, Oka GU, Souza DP, Cenens W, Bayer-Santos E, Matsuyama BY, Bueno NF, dos Santos TR, Alvarez-Martinez CE, Salinas RK et al (2019) Bacteria-killing type IV secretion systems. *Front Microbiol* 10: 1078
- Shneider MM, Buth SA, Ho BT, Basler M, Mekalanos JJ, Leiman PG (2013) PAAR-repeat proteins sharpen and diversify the type VI secretion system spike. *Nature* 500: 350–353
- Silverman JM, Austin LS, Hsu F, Hicks KG, Hood RD, Mougous JD (2011) Separate inputs modulate phosphorylation-dependent and -independent type VI secretion activation. *Mol Microbiol* 82: 1277–1290
- Skerniškytė J, Karazijaitė E, Deschamps J, Krasauskas R, Briandet R, Sužiedėlienė E (2019) The mutation of conservative Asp268 residue in the peptidoglycan-associated domain of the OmpA protein affects multiple *Acinetobacter baumannii* virulence characteristics. *Molecules* 24: 1972
- Sklar JG, Wu T, Gronenberg LS, Malinverni JC, Kahne D, Silhavy TJ (2007) Lipoprotein SmpA is a component of the YaeT complex that assembles outer membrane proteins in *Escherichia coli*. *Proc Natl Acad Sci USA* 104: 6400–6405
- Smith WPJ, Brodmann M, Unterweger D, Davit Y, Comstock LE, Basler M, Foster KR (2020) The evolution of tit-for-tat in bacteria via the type VI secretion system. *Nat Commun* 11: 5395
- Söding J (2005) Protein homology detection by HMM–HMM comparison. *Bioinformatics* 21: 951–960
- Souza DP, Oka GU, Alvarez-Martinez CE, Bisson-Filho AW, Dunger G, Hobeika L, Cavalcante NS, Alegria MC, Barbosa LRS, Salinas RK et al (2015) Bacterial killing via a type IV secretion system. *Nat Commun* 6: 1–9
- Stolle A-S, Meader BT, Toska J, Mekalanos JJ (2021) Endogenous membrane stress induces T6SS activity in *Pseudomonas aeruginosa*. *Proc Natl Acad Sci USA* 118: e2018365118
- Stutzmann S, Blokesch M (2020) Comparison of chitin-induced natural transformation in pandemic *Vibrio cholerae* O1 El Tor strains. *Environ Microbiol* 22: 4149–4166
- Szwedziak P, Pilhofer M (2019) Bidirectional contraction of a type six secretion system. *Nat Commun* 10: 1565
- The UniProt Consortium (2019) UniProt: a worldwide hub of protein knowledge. *Nucleic Acids Res* 47: D506–D515
- Thevenaz P, Ruttimann UE, Unser M (1998) A pyramid approach to subpixel registration based on intensity. *IEEE Trans Image Process* 7: 27–41

- Tiku V, Kofoed EM, Yan D, Kang J, Xu M, Reichelt M, Dikic I, Tan M-W (2021) Outer membrane vesicles containing OmpA induce mitochondrial fragmentation to promote pathogenesis of *Acinetobacter baumannii*. *Sci Rep* 11: 618
- Vesel N, Blokesch M (2021) Pilus production in *Acinetobacter baumannii* is growth phase dependent and essential for natural transformation. *J Bacteriol* 203: e00034-21
- Vettiger A, Basler M (2016) Type VI secretion system substrates are transferred and reused among sister cells. *Cell* 167: 99–110.e12
- Vettiger A, Winter J, Lin L, Basler M (2017) The type VI secretion system sheath assembles at the end distal from the membrane anchor. *Nat Commun* 8: 1–9
- Wang J, Brackmann M, Castaño-Díez D, Kudryashev M, Goldie KN, Maier T, Stahlberg H, Basler M (2017) Cryo-EM structure of the extended type VI secretion system sheath–tube complex. *Nat Microbiol* 2: 1507–1512
- Wang J, Brodmann M, Basler M (2019) Assembly and subcellular localization of bacterial type VI secretion systems. *Annu Rev Microbiol* 73: 621–638
- Waterhouse AM, Procter JB, Martin DMA, Clamp M, Barton GJ (2009) Jalview Version 2—a multiple sequence alignment editor and analysis workbench. *Bioinformatics* 25: 1189–1191
- Weber BS, Hennon SW, Wright MS, Scott NE, de Berardinis V, Foster LJ, Ayala JA, Adams MD, Feldman MF (2016) Genetic dissection of the type VI secretion system in *Acinetobacter* and identification of a novel peptidoglycan hydrolase, TagX, required for its biogenesis. *MBio* 7: e01253-16
- Wilharm G, Piesker J, Laue M, Skiebe E (2013) DNA uptake by the nosocomial pathogen *Acinetobacter baumannii* occurs during movement along wet surfaces. *J Bacteriol* 195: 4146–4153
- Wimley WC (2003) The versatile β -barrel membrane protein. *Curr Opin Struct Biol* 13: 404–411
- Wu T, Malinverni J, Ruiz N, Kim S, Silhavy TJ, Kahne D (2005) Identification of a multicomponent complex required for outer membrane biogenesis in *Escherichia coli*. *Cell* 121: 235–245
- Yin M, Yan Z, Li X (2019) Architecture of type VI secretion system membrane core complex. *Cell Res* 29: 251–253
- Yu M, Tsang JSH (2006) Use of ribosomal promoters from *Burkholderia cenocepacia* and *Burkholderia cepacia* for improved expression of transporter protein in *Escherichia coli*. *Protein Expr Purif* 49: 219–227
- Zimmermann L, Stephens A, Nam S-Z, Rau D, Kübler J, Lozajic M, Gabler F, Söding J, Lupas AN, Alva V (2018) A completely reimplemented MPI bioinformatics toolkit with a new HHpred server at its core. *J Mol Biol* 430: 2237–2243
- Zoued A, Durand E, Bebeacua C, Brunet YR, Douzi B, Cambillau C, Cascales E, Journet L (2013) TssK is a trimeric cytoplasmic protein interacting with components of both phage-like and membrane anchoring complexes of the type VI secretion system. *J Biol Chem* 288: 27031–27041



License: This is an open access article under the terms of the Creative Commons Attribution-NonCommercial-NoDerivs 4.0 License, which permits use and distribution in any medium, provided the original work is properly cited, the use is non-commercial and no modifications or adaptations are made.